Scientific Research Publishing

Materials Sciences and Applications, 2025, 16(8), 453-480
https://www.scirp.org/journal/msa
ISSN Online: 2153-1188
ISSN Print: 2153-117X

Performance of Lammelar Zirconium Phosphate as Flame Retardant for Post-Consumer Poly (Ethylene Terephthalate)

Gerson Alberto Valencia Albitres[1*], Enzo Erbisti Garcia[1], Carlos Magno Fialho Soares[1], Daniela de França da Silva Freitas[1], Michelle Gonçalves Mothé[2], Sibele Piedade Cestari[3], Luis Claudio Mendes[1]

[1]Instituto de Macromoléculas Professora Eloisa Mano, Universidade Federal do Rio de Janeiro, Rio de Janeiro, Brazil
[2]Escola de Química, Universidade Federal do Rio de Janeiro, Rio de Janeiro, Brazil
[3]Innovation in Polymer Engineering (PIEP), University of Minho, Guimarães, Portugal
Email: *gvalenciaa@ima.ufrj.br

How to cite this paper: Albitres, G.A.V., Garcia, E.E., Soares, C.M.F., da Silva Freitas, D.F., Moth, M.G., Cestari, S.P. and Mendes, L.C. (2025) Performance of Lammelar Zirconium Phosphate as Flame Retardant for Post-Consumer Poly (Ethylene Terephthalate). *Materials Sciences and Applications*, **16**, 453-480.
https://doi.org/10.4236/msa.2025.168026

Received: June 25, 2025
Accepted: August 23, 2025
Published: August 26, 2025

Abstract

Due to the damage caused to human lives and financial losses, there is a global concern about materials that offer greater fire resistance. This research investigated the action of the lammelar zirconium phosphate (ZrP) as flame retardant (FR) when added in post-consumer poly(ethylene terephthalate) named as rPET. ZrP was tested alone and in combination with aluminum hydroxide [$Al(OH)_3$] and sodium hypophosphite [$NaPO_2H_2{\cdot}H_2O$]. PET beverage bottles were collected, washed, shredded as flakes and ground. Firstly, masterbatches of rPET/FR (80/20 wt./wt.%) were processed in co-rotating twin-screw extruder, processing window 120 - 260˚C, at 300 rpm. The addition of each flame retardant altered the domain distribution curve and relaxation time of rPET. The presence of flame retardant did not modify the X-ray diffraction pattern of rPET. Calorimetric data indicated that the flame retardants increased the cooling crystallization temperature, while their effects on melting temperature and degree of crystallization varied depending on the specific retardant system. Rheology showed that storage and loss moduli varied with the kind of flame retardant and that rPET changed the behavior from Newtonian to pseudoplastic. Finally, composites of rPET/masterbatch (75/25 wt./wt.%) were processed in a mixing chamber, at 260˚C, 60 rpm for 6 minutes. Compression moulding specimen was prepared for flammability test. Field emission scanning electron microscopy and energy dispersive spectroscopy revealed that ZrP nanoparticles were better dispersed and distributed in the specimen when compared to the microparticles of $Al(OH)_3$ and $NaPO_2H_2{\cdot}H_2O$. ZrP

showed the best dripping speed and flame extinguishing time.

Keywords

rPET, Zirconium Phosphate, Aluminum Hydroxide, Sodium Hypophosphite, Flame Retardancy, Sustainability

1. Introduction

Plastic products are indelibly rooted in modern society. However, most of them are randomly discarded in nature, causing serious damage to the environment and polluting terrestrial ecosystems, groundwater, and aquatic biomes. There is widespread concern about preserving the planet [1]-[3]. Owing to the problems caused by solid waste pollution and considering the enormous energy potential concentrated in the different types of discarded plastics, polymer recycling should be considered an effective solution to minimize the environmental impact of plastic disposal [4]-[8]. Whether applied as commodity plastic or engineering plastic, polyethylene terephthalate (PET), along with polyolefins, is among the most widely used plastics around the world [9]. In 2018, about 20 million tons of food-grade PET bottles were manufactured, but only 845 thousand tons were recycled. In the coming years, it is expected that around 3 million tons will be mechanically recycled [10] [11]. Shirazimoghaddam *et al.* studied the chemical recycling (depolymerization) of PET in the presence of a niobium catalyst. A high yield of BHET (2-hydroxyethyl terephthalate) precursor and oligomers, considered suitable for repolymerization, was obtained [12]. Giraldo-Narcizo *et al.* experienced the depolymerization of PET using alkaline pretreatment and temperature. The process presented advantages such as higher yield than other technologies [13]. Pu *et al.* synthesized polyurethane elastomer using PET depolymerized from post-consumer bottles as a chain extender. The authors noted the high transparency and extensibility of the final product [14]. Ghosh *et al.* published a study projecting the feasibility of recycling PET bottles for the period 2020-2049. In the study, they emphasized that both chemical and secondary recycling (from selective collection) should improve the circularity of PET bottles and reduce carbon footprints, replacing the manufacture of virgin PET [15]. Lerna *et al.* studied the effect of recycled PET bottles as plastic aggregates on the improvement of concrete ductility. Reduction of heat conduction capacity and limited decrease of compressive strength were reported [16]. Roungpaisan *et al.* conducted a comparative study on recycled filaments derived from PET bottles and PET knitted fabrics. The latter produced a fiber with good formability and better melting spinning, along with additional improvement of thermal and mechanical properties [17]. As a material of fossil origin, plastics are potentially combustible materials. A survey carried out in the USA and European Union revealed a high rate of deaths, injuries and significant financial losses due to residential building fires. In this context, the addi-

tion of flame retardants to plastic formulations is a way to prevent human and financial losses [18]. Fire retardants have gained public interest for the last 30 years owing to their increased importance on personnel safety. Many flame-retardant additives, such as halogen-based, phosphorus-based, metal oxides, and mineral fillers have been used as a measure of fire retardancy plastics [19]-[22]. Aluminum hydroxide $Al(OH)_3$ has been used in various sectors. Shi *et al.* investigated a new flame retardant for poly(ethylene terephthalate) (PET) based on hydroxyethyl diphosphate modified with different particles sizes of aluminum hydroxide. The best result was attained by particle size of 10 μm which was ascribed to the combined effects namely decomposition of phosphoric acid and dehydration of $Al(OH)_3$ [23]. Park *et al.* highlighted the application of $Al(OH)_3$ as flame retardant for being environmentally friendly, free of acid and halogen [24]. Hypophosphites have also been used as a potential flame retardant for polyerster. Yang *et al.* reported that the addition of 10 wt.% of aluminum hypophosphite in composites of polyethylene terephthalate/glass fiber attained high limited oxygen index and V-0 classification in UL-94 test [25]. The synergistic effect of the mixing of diethylzinc hypophosphite (ZDP) and nano-SiO_2 as flame retardant for PET was investigated by Zheng and collaborators. The additivation of PET induced classification V-0 for vertical combustible grade and increased its limiting oxygen index from 21% to 30%. The nano-SiO_2 imputed better dripping behavior [26]. Composite of poly(butylene terephthalate)/ glass fiber was composed with rare earth hypophosphite and melamine cyanurate as flame retardants. The authors registered that the mixing induced slight decrease of the thermal stability, reduction in heat release rate and limiting oxygen index [27]. Assocition of maleic anhydride and sodium hypophosphite as flame retardant for cotton finishing was evaluated by Wu and Yang. It was revealed that the treatment with this combination reduced the flammability of cotton fleece from the Class III to Class I and it was considered low cost matter [28]. Considering the special properties—ion exchange capacity, ion intercalation, ionic conductivity, catalytic activity—of the lammelar phosphates and the expertise of our research group in the synthesis and new applications of zirconium and titanium phosphates [29] [30], the proposal of this research was to evaluate the effectiveness of ZrP alone and in combination with aluminum hydroxide and sodium hypophosphite as potential flame retardant for post-consumer poly(ethylene terephthalate) (rPET).

2. Experimental

2.1. Material

Post-consumer bottles of poly(ethylene terephthalate) (rPET) from the Macromolecules Institute community were used. Zirconium phosphate, phosphoric acid (H_3PO_4, 85 % wt./mL, Vetec), zirconium (IV) oxide chloride ($ZrOCl_2.8H_2O$, Sigma-Aldrich), octadecylamine (Oct, Sigma-Aldrich) and absolute ethanol (99 %) were purchased. Aluminum hydroxide [$Al(OH)_3$, Isofar] and sodium hypophosphite ($NaPO_2H_2{\cdot}H_2O$, Isofar) were acquired. All reagents were used as re-

ceived.

2.2. Post-Consumer Bottles of Poly (Ethylene Terephthalate) (rPET) Treatment

Post-consumer PET bottles were collected from the Macromolecules Institute community. The labels were removed. The bottles were washed with water plus light detergent, rinsed only with water and dried. Following, they were cut into flakes and then ground.

2.3. Synthesis and Modification of Lammelar Zirconium Phosphate (ZrP)

The lammelar ZrP was synthesized following its intercalation with octadecylamine (Oct:ZrP, 2:1) as reported elsewhere [31]. The intercalation with octadecylamine aimed at improving the dispersibility between ZrP and its counterparts.

2.4. Masterbatch, Composite and Flammability Specimen Preparation

The following masterbatches were prepared: rPET/ZrP (80/20 wt./wt.%); rPET/$Al(OH)_3$/$NaPO_2H_2{\cdot}H_2O$ (80/10/10 wt./wt./wt.%) and rPET/ZrPOct/$Al(OH)_3$/$NaPO_2H_2{\cdot}H_2O$ (80/10/5/5 wt./wt./wt./wt.%) and they were processed in a Teck Tril co-rotating twin-screw extruder (L/D = 36, screw diameter = 22 mm), processing window 120 - 260˚C, at 300 rpm. Samples were labelled as rPET, rPET/ZrP, rPET/$Al(OH)_3$/$NaPO_2H_2{\cdot}H_2O$ and rPET/ZrPOct/$Al(OH)_3$/$NaPO_2H_2{\cdot}H_2O$ (**Figure 1**). Composites of rPET/masterbatch (75/25 wt./wt.%) were processed in a Haake Rheocord 9000 torque rheometer at 260=˚C, 60 rpm for 6 minutes. The specimens for flammability test were prepared by compression moulding in a Carver press at 260°C, 5,000 psi. Following, the specimens were cooled at 180˚C C for 2 minutes and finally cooled in a cooling plate, at 20˚C, for 3 minutes. The specimens were identified as FS1 (rPET), FS2 (rPET/ZrP)—represent 5 wt. % of ZrP-, FS3 (rPET/$Al(OH)_3$/$NaPO_2H_2{\cdot}H_2O$)—represent 2.5 wt. % for each one—and FS4 (rPET/ZrPOct/$Al(OH)_3$/$NaPO_2H_2{\cdot}H_2O$)—represent 2.5 wt. % for ZrP, and singly 1.25 wt. % for $Al(OH)_3$ and $NaPO_2H_2{\cdot}H_2O$.

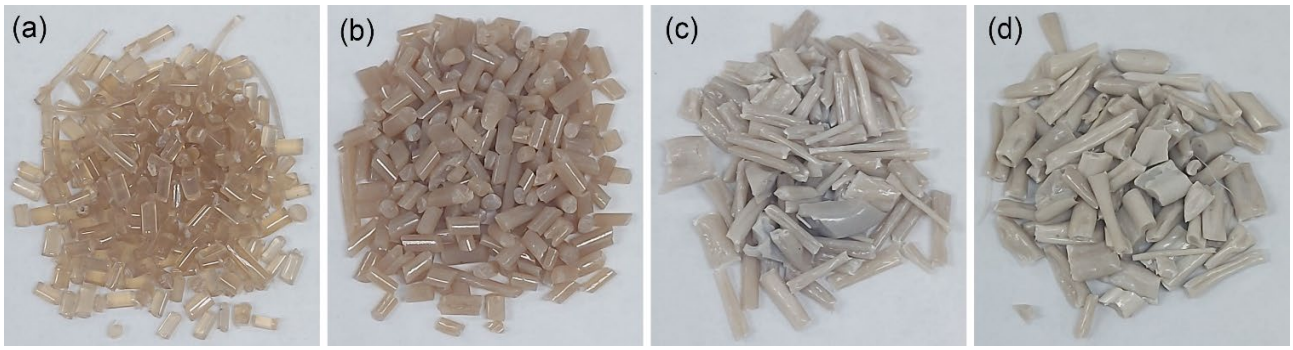

Figure 1. Images of masterbatches after processing: (a) rPET, (b) rPET/ZrP, (c) rPET/$Al(OH)_3$/$NaPO_2H_2{\cdot}H_2O$ and (d) rPET/ZrPOct/$Al(OH)_3$/$NaPO_2H_2{\cdot}H_2O$.

2.5. Fourier Transform Infrared Spectroscopy (FTIR)

The infrared analysis was performed in a Perkin Elmer Frontier model instrument, covering the range from 4000 to 500 cm^{-1}, with 60 scans and a resolution of 4 cm^{-1}, using KBr disk.

2.6. Raman Spectroscopy

The Raman spectroscopy was performed using a Raman Microscope equipped with a laser, at a wavelength of 532 nm and a 50x lens, in the range of 4000-200 cm^{-1}. The vibrational modes were evaluated.

2.7. Time-Domain Hydrogen Nuclear Magnetic Resonance (TDHNMR)

Time domain hydrogen nuclear magnetic resonance was accomplished in a Maran Ultra 23 equipment with hydrogen nucleus pulse sequence, equipped with a probe of 18 mm, operating at a frequency of 23 MHz, at 30˚C. The domain distribution curve was acquired, and the relaxation time was determined.

2.8. Wide Angle X-Ray Diffraction (WAXD)

The crystallographic aspect of each sample was monitored in a Rigaku Ultima IV diffractometer with CuKα radiation (λ = 1.5418 Å), 40 kV, 20 mA, a step of 0.05, ranging the 2θ angle from 2˚ to 50˚.

2.9. Thermogravimetry (TGA)

In TA equipment model Q500 the TGA analysis was performed at a range of 30-700˚C, at 10˚C·min^{-1} and nitrogen as carrying gas. Mass loss and derivative curves were assessed. The degradation temperature was evaluated.

2.10. Differential Scanning Calorimetry (DSC)

The calorimetry tests were performed in DSC1 STARe SYSTEM following the recommendations specified by ASTM D3418 [32]. Three cycles were conducted: firstly, heating from 30 to 280˚C at a rate of 10˚C /min, followed by cooling from 280 to 30˚C at the same rate, and finally, another heating cycle identical to the first. For each sample, the crystallization (T_c) and melting (T_m) temperatures were pointed out, as well as the degree of crystallization (X_c) determined through the ratio of PET experimental melting enthalpy (ΔH_{sample}) and the 100% crystalline PET (ΔH_{ref}, 130 J·g^{-1}), considering $X_c = (\Delta H_{sample} / \Delta H_{ref}) \cdot (1 - \Phi)$, where Φ is the filler weight fraction in each composite [33].

2.11. Rheology

The parallel plate rheology was conducted in TA rheometer, model AR-2000, with a geometry of 25 mm diameter, at 260˚C, strain amplitude of 10^{-3}, from 10^{-1} to 10^{3} rad/s. The complex moduli (storage and loss) and complex viscosity were determined.

2.12. Field Emission Scanning Electron Microscopy (FESEM) and Energy Dispersive Spectroscopy (EDS)

Flammability specimens were evaluated by field emission scanning electron microscopy and energy dispersive spectroscopy analysis. A Tescan FESEM model MIRA 4 LMU (LowVac Mode UniVac™) equipment accoupled with an EDS detector (30 mm^2 Si_3N_4 window, resolution lower than 129 eV, MnKα emission line) enabled the viewing of the dispersion and distribution of main elements (zirconium, aluminum, sodium) in each type of flame retardant.

2.13. Flammability Tests

The flammability test was performed following the ASTM D635-22 [34] using a Bunsen burner and propane/butane gas mixture. Dripping speed, flame extinguishing time, and ignition time were assessed, with the average and standard deviation calculated from three measurements. The whole test was registered by video.

3. Results and Discussion

3.1. Infrared Spectroscopy

Figure 2 shows the infrared spectra of the flame retardants in different spectral regions. The ZrP presented absorptions at 3594 and 3509 cm^{-1} (P-O-H and water hydrogen bond); 3151 cm^{-1} (O-H axial stretching of water hydrogen bond); 1619 cm^{-1} (water hydrogen bond at crystalline lattice); 1250, 1049 and 967 cm^{-1} (PO_4^{2-} stretching); 594 and 532 cm^{-1} (P-O of PO_4^{3-} asymmetric bending) in agreement with several works [31] [35] [36]. The $Al(OH)_3/NaPO_2H_2{\cdot}H_2O$ displayed absorptions at 3439 cm^{-1} (O-H stretching of hydrogen bonds); 2346 cm^{-1} (P-H stretching), 1644 cm^{-1} (H-O-H bending); 1582 cm^{-1} ($Al\text{-}OH_3$); 1173 cm^{-1} (P-H scissor bending); 1089 cm^{-1} (P-H wag bending); 1045 cm^{-1} ($P\text{-}O_2$ symmetric stretching); 955 cm^{-1} (O-H stretching); 817 cm^{-1} (P-H rocking motion, asymmetric stretching); 690 cm^{-1} (Al-O skeleton vibrations); 545 cm^{-1} (Al-O-H-Al translational vibrations) and 478 cm^{-1} ($P\text{-}O_2$ scissor bending) in agreement with several authors [37]-[45]. The $ZrPOct/Al(OH)_3/NaPO_2H_2{\cdot}H_2O$ displayed bands at 3427 cm^{-1} (O-H stretching); 2959; 2919 and 2851 cm^{-1} (C-H of CH_3 stretching); 2353 cm^{-1} (P-H stretching); 1641 cm^{-1} (O-H hydrogen bonding, stretching); 1584 cm^{-1} ($AlOH_3$); 1469 cm^{-1} (N-H of NH_3^+ vibration, octadecylamine); 1397 cm^{-1} ($Al\text{-}OH_3$); 1164 cm^{-1} (P-H scissoring); 1089, 1042 cm^{-1} ($P\text{-}O_3$ asymmetric stretching) and 975 cm^{-1} (P-O-H symmetric stretching); 819 cm^{-1} (P-H rocking motion, asymmetric stretching); 721 cm^{-1} (CH_2 vibration of octadecylamine) and 545 cm^{-1} (($P\text{-}O_3$) asymmetric and Al-O-H-Al translational vibrations). Although in equivalent amounts, the spectra of the combination of the three flame retardants indicated that all spectral regions are dominated by the absorptions of $Al(OH)_3/NaPO_2H_2{\cdot}H_2O$. Table 1 highlights the samples along with the main absorptions of each flame retardant, as well as the studies that support the attributions mentioned herein. Figure 3 displays the spectra of rPET and masterbatches at various spectral

regions. The rPET displayed bands at 3435 (O-H end groups stretching); 3104 (water O-H stretching); 3081 (ring C-H stretching); 2964 and 2917 (aliphatic C-H stretching); 2629 (O-H stretching; C=O carbonyl group); 2532 (C=C stretching); 2386 and 2286 (H-C=C and carbonyl stretching); 2102 (C=C stretching); 1952 (C=O stretching); 1719 (C=O ester stretching); 1637 and 1615 (aromatic C-C bending); 1579 and 1505 (C=C stretching); 1456 and 1,410 (aromatic skeletal stretching); 1372 and 1342 (-CH_2 gauche wagging and -CH_2 trans wagging); 1244 (O=C-O asymmetric stretching); 1175 (C-O-C stretching); 1098 (C-O symmetric stretching); 1043 (C-O vibration); 1017 (aromatic C-H in plane bending); 972 (O-CH_2 stretching); 873 (aromatic C-H stretching); 794 (aromatic C-H bending); 725 and 632 cm^{-1} (aromatic C-H out of plane stretching)

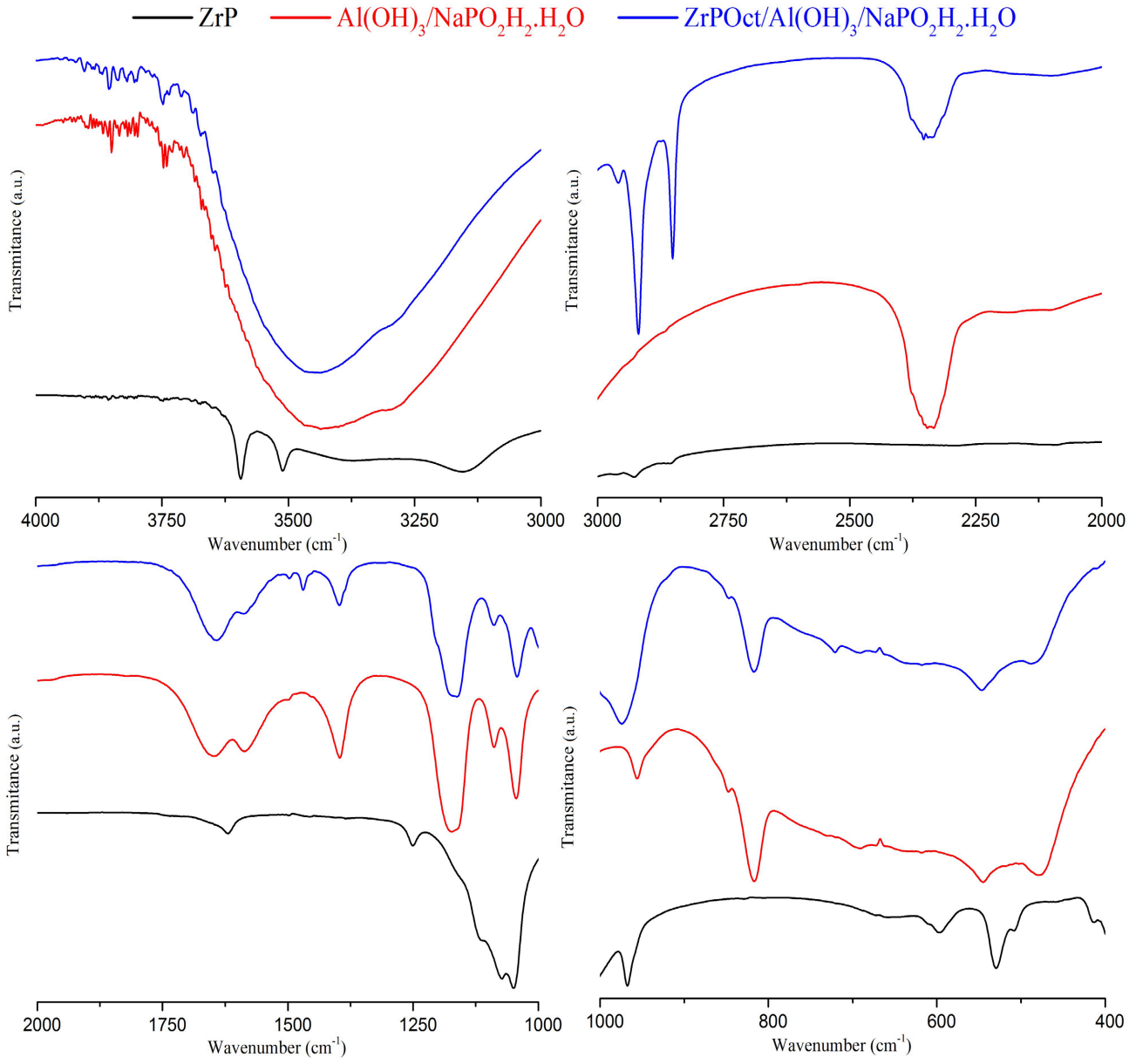

Figure 2. Spectra of flame retardants at different spectral regions.

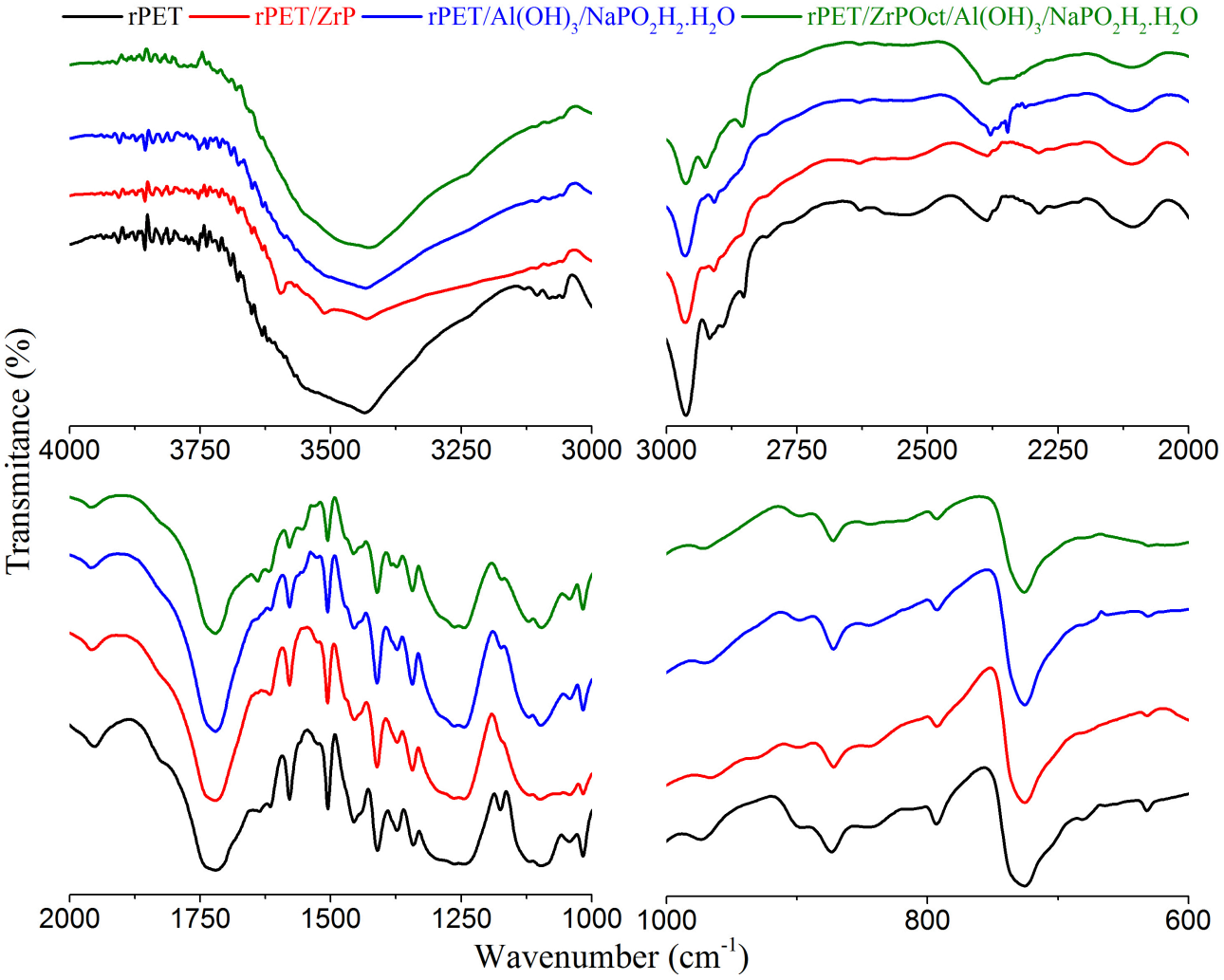

Figure 3. Spectra of rPET and masterbatches at different spectral regions.

Table 1. Summary of samples and absorptions.

Sample	Absorption/cm^{-1}	Reference
ZrP	3594; 3509; 3151; 1619; 1049; 967; 594; 532	[30] [35]
$Al(OH)_3/NaPO_2H_2{\cdot}H_2O$	3439; 2346; 1644; 1582; 1498; 1173; 1089; 1045; 955; 817; 690; 545; 478	[36]-[42] [44]
$ZrPOct/Al(OH)_3/NaPO_2H_2{\cdot}H_2O$	3427; 2959; 2919; 2851; 2353; 1641; 1584; 1469; 1397; 1164; 1089; 1042; 975; 819; 721; 545	[30] [35]-[42] [44]

[46]-[48]. Absorptions of rPET/ZrP were assigned at 3595; 3510; 3431; 2965; 2909; 2629; 2532; 2386; 2286; 2106; 1722; 1615; 1579; 1505; 1456; 1410; 1372; 1342; 1244; 1098; 1042; 1016; 966; 872; 792; 726 cm^{-1}. rPET/$Al(OH)_3/NaPO_2H_2{\cdot}H_2O$ absorptions were registered at 3435; 2964; 2908; 2379; 2347; 2313; 2109; 1960; 1719; 1615; 1579; 1505; 1455; 1411; 1373; 1344; 1241; 1173; 1120; 1098; 1042; 1017; 972; 898; 873; 845; 793; 662; 631 cm^{-1}. The rPET/$ZrPOct/Al(OH)_3/NaPO_2H_2{\cdot}H_2O$ absorptions appeared at 3420; 2963; 2922; 2855; 2381; 2110; 1960; 1719; 1640; 1618; 1579; 1554; 1505; 1456; 1410; 1373; 1344; 1262; 1244; 1172; 1120; 1095; 1043; 1017; 972;

898; 872; 843; 794; 725; 631 cm^{-1}. A more careful observation of the masterbatches' spectra showed that in each spectral region, their contour closely resembles that of rPET, although some specific flame retardant absorptions can be visualized. In summary, no significant changes were observed in the spectra, indicating the absence of chemical interaction between the components.

3.2. Raman Spectroscopy

Figure 4 depicts Raman spectra of flame retardants. The ZrP disclosed Raman shift at 3509 cm^{-1} (H-O-H stretching); 3135 cm^{-1} (P-O-H stretching); 1622 and 1616 cm^{-1} (O-H stretching water at crystalline lattice), 1071 and 1037 cm^{-1} (orthophosphate group) and 962 cm^{-1} (pyrophosphate group) as published by He and collaborators [49]. The $Al(OH)_3/NaPO_2H_2{\cdot}H_2O$ showed Raman shift at 3421 cm^{-1} (O-H stretching); 2355 cm^{-1} (P-H symmetric stretching); 1159 cm^{-1} (P-H scissor); 1072 cm^{-1} (P-H wagging); 1055 cm^{-1} (Al-O-H symmetric and asymmetric stretching); 928 cm^{-1} (P-H twisting); 649 cm^{-1} (Al cluster vibration); 551 cm^{-1} (Al-O-Al deformation) as registered by Frost *et al.* [40] and Tsuboi and collaborators [50]. The $ZrPOct/Al(OH)_3/NaPO_2H_2{\cdot}H_2O$ exhibited Raman shift at 2880 and 2847 cm^{-1} (C-H symmetric stretching of CH_3 and CH_2 in octadecylamine); 2355 and 2329 cm^{-1} (P-H symmetric and asymmetric stretching); 1295 cm^{-1} (tetrahedral PO_4 symmetric stretching); 1169 cm^{-1} (P-H scissoring); 1128 cm^1 (C-H_3 stretching); 1098 cm^{-1} (P-H wagging); 1073 cm^{-1} (P-O_2 symmetric stretching); 1062 cm^{-1} (tetrahedral P-O_4 symmetric stretching); 1002 (P-O_4 symmetric stretching); 929 cm^{-1} (P-H twisting); 825 cm^{-1} (P-H rocking); 473 cm^{-1} (P-O_2 scissoring) and 426 cm^{-1} (PO_4^- torsional vibration) in agreement with Xavier and Nayar [40] and by Darkhalil and collaborators [51]. **Figure 5** shows the Raman spectra of rPET and masterbatches. A significant rPET Raman shift can be noticed at 3083 cm^{-1} (aromatic C-H stretching); 2966 cm^{-1} (C-H stretching of glycol CH_2); 1726 cm^{-1} (C=O stretching); 1614 cm^{-1} (aromatic C=C stretching); 1451 cm^{-1} (C-H deformation); 1412 cm^{-1} (aromatic C-C stretching); 1371 cm^{-1} (C-H_2 wagging); 1288 cm^{-1} (aromatic C-C stretching and C-O stretching); 1177 cm^{-1} (aromatic C-H in plane bending); 1118 cm^{-1} (aromatic C-C stretching and C-O stretching); 1098 cm^{-1} (C-O-C asymmetric stretching); 1001 cm^{-1} (C-C stretching); 858 cm^{-1} (aromatic C-C stretching and C-O stretching); 794 cm^{-1} (aromatic CH out of plane bending); 703 cm^{-1} (aromatic C-C stretching); 632 cm^{-1} (aromatic C-C=C in plane bending) and 276 cm^{-1} (aromatic C-C stretching and C-C=C bending) in agreement with Bistricic *et al.* [52], Zhu *et al.* [53] and Peñalver and collaborators [54]. Regarding the rPET/ZrP, the Raman shifts at 3082; 2965; 1727; 1615; 1445; 1410; 1290; 1183; 1092; 1000; 857; 794; 701; 631 and 280 cm^{-1} were associated to rPET, while vibrational mode at 1054 cm^{-1} coupled with 1071 and 1037 cm^{-1} were attributed to ZrP vibrations. The vibrational modes of $rPET/Al(OH)_3/NaPO_2H_2{\cdot}H_2O$ at 3082; 2964; 2907; 1727; 1615; 1463; 1414; 1375; 1290; 1183; 1117; 1095; 1000; 858; 795; 702; 632 and 278 cm^{-1} were assigned to rPET. For $rPET/ZrPOct/Al(OH)_3/NaPO_2H_2{\cdot}H_2O$ at 3082; 2966; 2909; 1726; 1614; 1458; 1414; 1377; 1289; 1177; 1116; 1095; 1002; 857; 794; 702; 632 and

277 cm^{-1} were associated to rPET. Herein, no chemical interaction was observed in the mixing of three flame retardants. Additionally, the spectra of the composites in any spectral region closely resemble those of rPET. The results are consistent with those obtained from FTIR analysis.

3.3. Time-Domain Hydrogen Nuclear Magnetic Resonance (TDHNMR)

Domain distribution curves are shown in **Figure 6**. Two relaxation regions with high (below 5×10^3 ms) and low (between 450 – 1250×10^3 ms) molecular mobility are observed in pure rPET. With the addition of ZrP, the high mobility region of rPET shifts to higher relaxation times, showing increased intensity, and a new region emerges between 50 - 60 $\times$ 10^3 ms. The domain at higher relaxation time showed no change. A similar behavior was observed when the $Al(OH)_3/NaPO_2H_2{\cdot}H_2O$ was added.

Domains with higher molecular mobility exhibited shorter relaxation times compared to those for ZrP. On the contrary, the domain with lower molecular mobility was enlarged and shifted to higher relaxation times. Also, the ZrPOct/$Al(OH)_3/NaPO_2H_2{\cdot}H_2O$ showed a tendency towards lower relaxation times, although the decrease was less pronounced than in the two previous cases. No change was noticed for the domain with higher relaxation times. Xerogels of

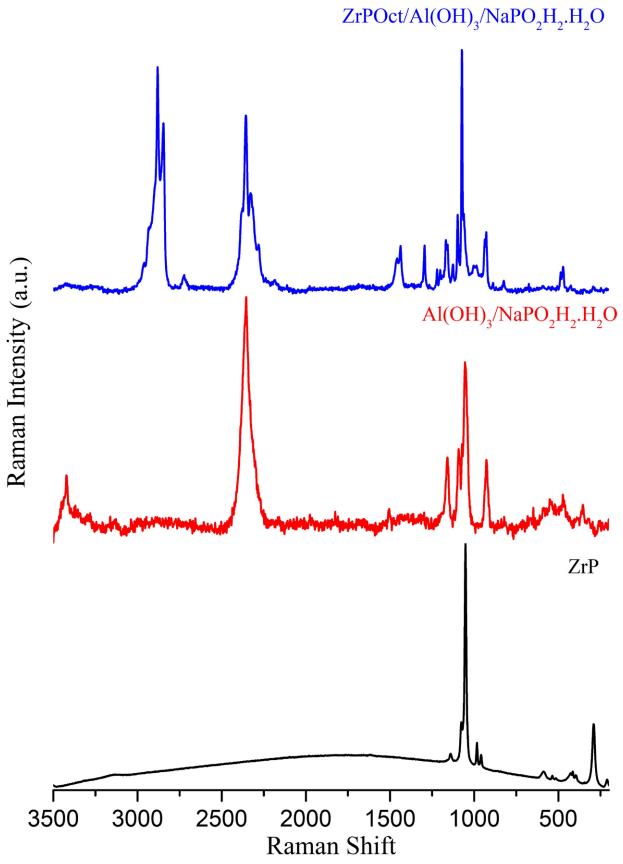

Figure 4. Raman spectra of flame retardants.

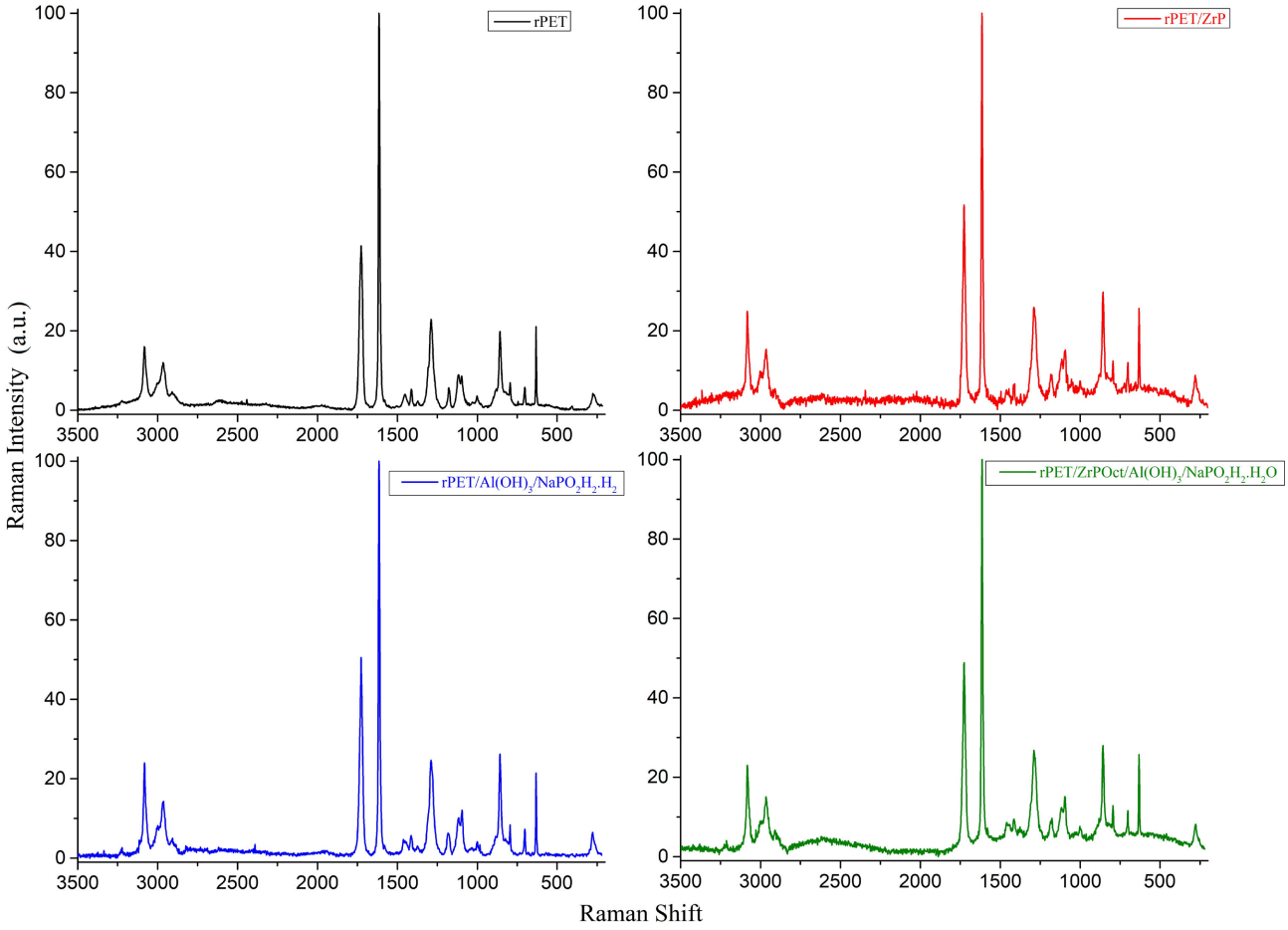

Figure 5. Raman spectra of rPET and masterbatches.

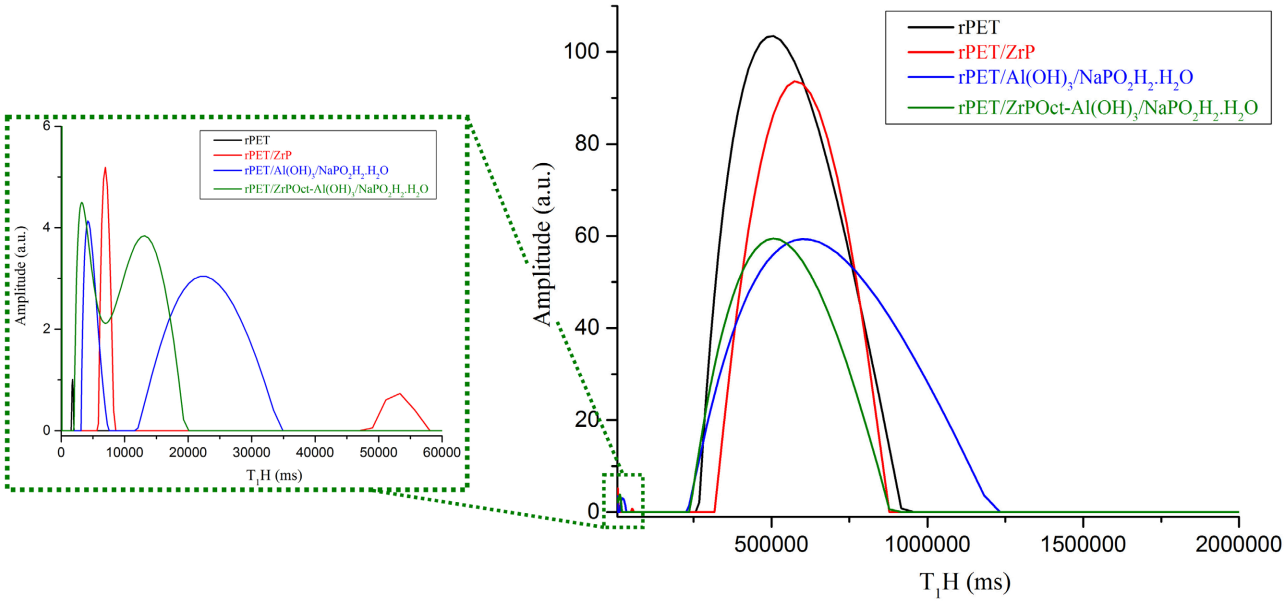

Figure 6. Domain distribution curves of the rPET and masterbatches.

poly (vinyl alcohol) (PVA) filled with silica nanoparticle (SiO_2) were studied by

Rodrigues and collaborators. Through time domain nuclear magnetic resonance, it was noticed that SiO_2 altered the PVA molecular mobility although there was not chemical interaction between them [55]. In general, all flame retardants showed some effect on the molecular mobility of rPET. It was assumed that the shift of the relaxation time and the enlargement of domains could be associated with the dispersion and distribution of flame retardants within the two relaxation regions of rPET.

3.4. X-Ray Diffraction

Figure 7 displays the diffraction pattern of the flame retardants. The ZrP showed diffraction angles at 12.3 (*hkl* plane), 20.4, 25.6, 34.6, 38 and 48.6˚, as reported by Mendes and collaborators [31]. The main $Al(OH)_3$ diffraction angles at 14.5-15.7 (020)*, 18.9 (002)**, 20.6 (200)**, 28.2 (120)*, 32.2, 38.3 (031)*, 40.7 and 49˚ (200)* are representative of the mixing of its crystalline forms—boehmite (orthorhombic)* and gibbsite (monoclinic)**, as reported by Bian and co-authors [37]. The $NaPO_2H_2{\cdot}H_2O$ showed the main diffraction angles at 11, 14.5, 15.2, 27.2, 28.7,

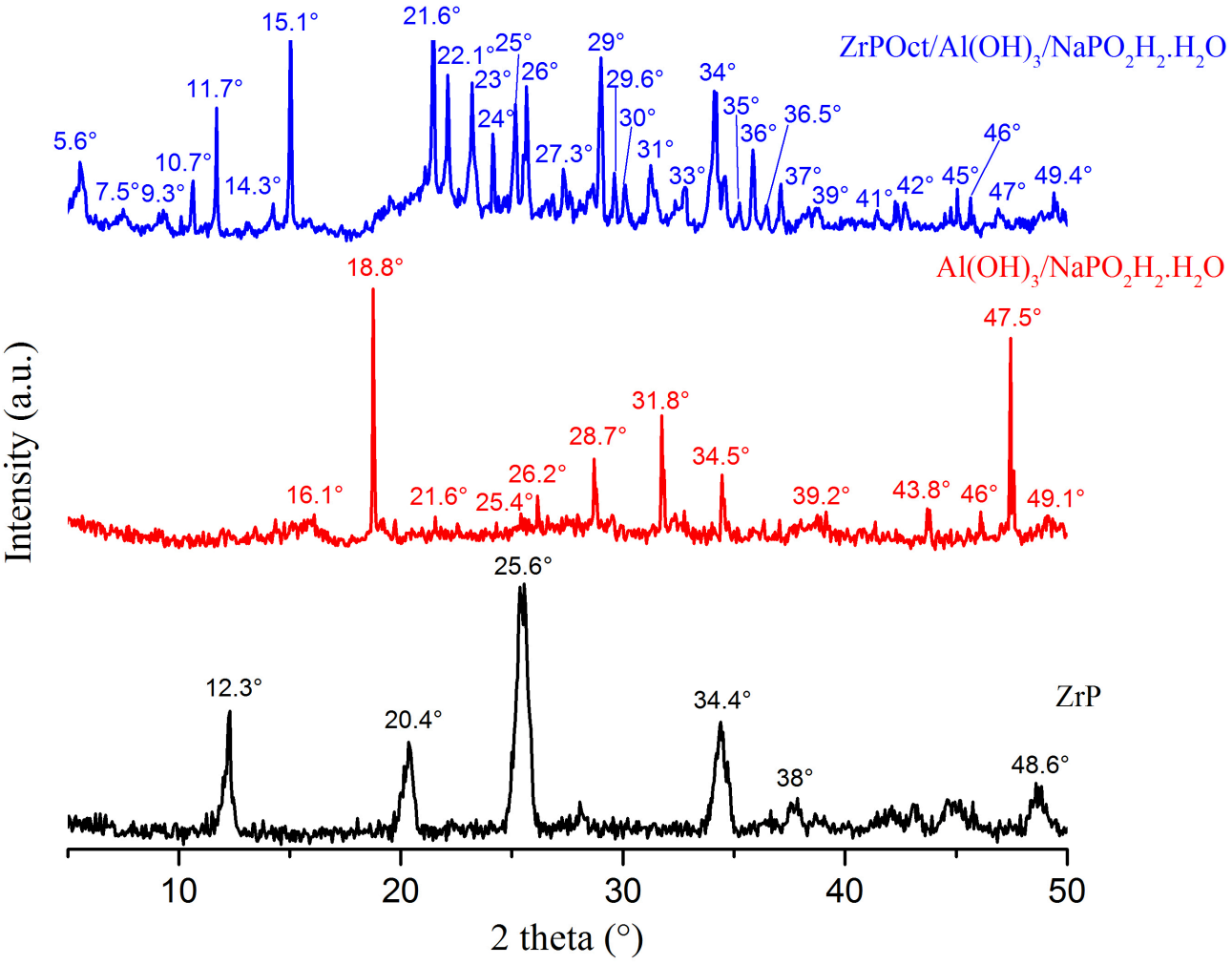

Figure 7. Diffraction pattern of the flame retardants.

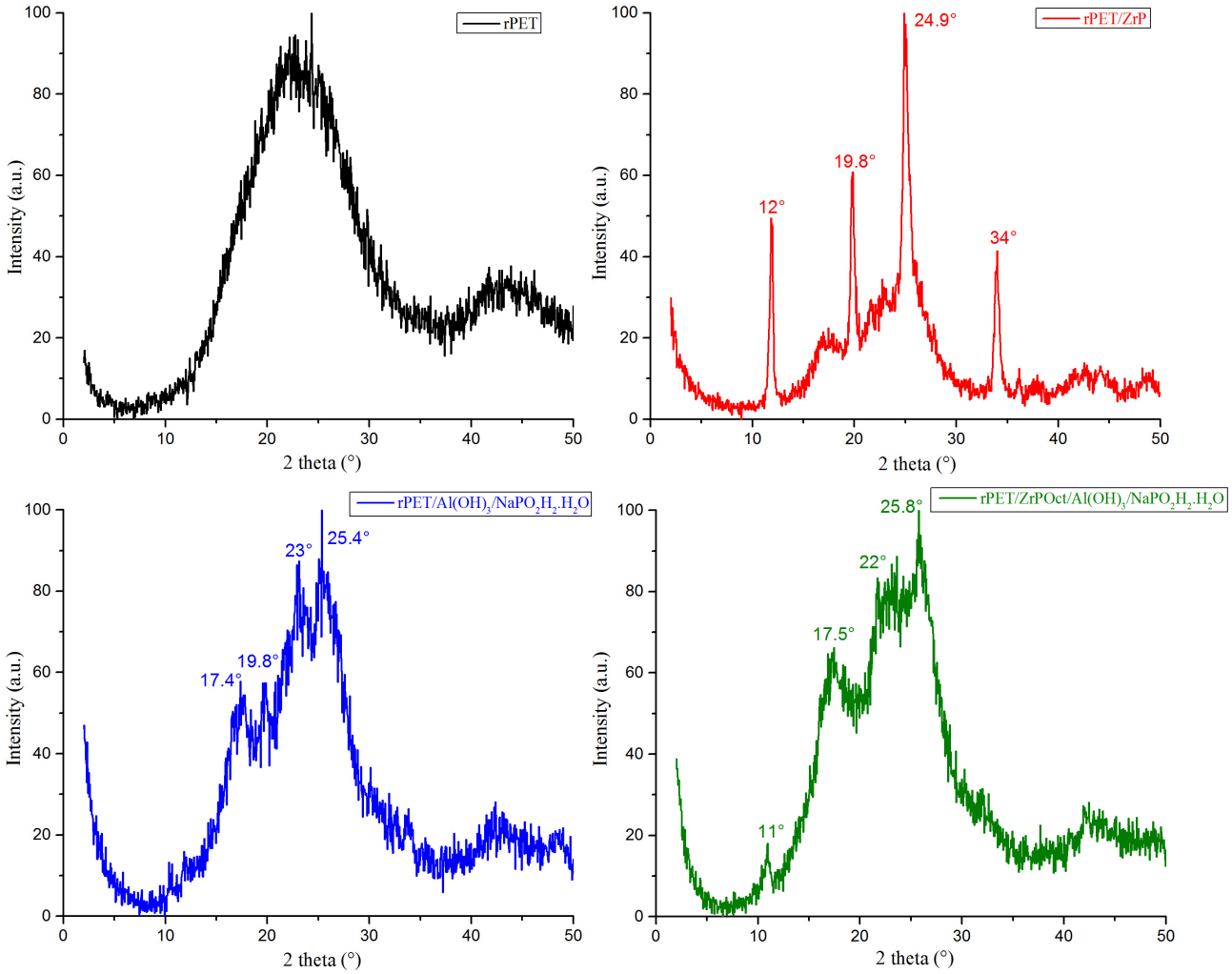

Figure 8. Diffraction pattern of the rPET and masterbatches.

30.4, 31.7, 34.9, 41.7 and 47.3˚, which are attributed to different crystalline planes [52]. The $Al(OH)_3/NaPO_2H_2{\cdot}H_2O$ diffraction angles appeared at 16.1, 18.8*, 21.6, 25.4, 26.2, 28.7**, 31.8*, 34.5**, 39.2, 43.8*, 46*, 47.5** and 49.1˚. The $ZrPOct/Al(OH)_3/NaPO_2H_2{\cdot}H_2O$ diffraction angles appeared at 4, 5.6, 7.5, 9.3, 10.7*, 11.7*, 14.7, 15.1*, 21.6*, 22.1*, 23*, 24*, 25*, 26*, 27.3, 29*, 29.6, 30, 31, 33, 34*, 35, 36**, 36.5**, 37**, 39**, 41*, 42*, 45*, 46*, 47* and 49.4˚*. The diffraction peaks below 10˚ could be attributed to the intercalation in ZrPOct. The diffraction peaks (*) and (**) were attributed to aluminum hydroxide and sodium hypophosphite, respectively. **Figure 8** presents the X-ray diffractions of rPET and masterbatches. The rPET showed two amorphous halos around 23 and 44˚. This could be attributed to the effect of quenching during the extrusion process, as described by Albitres *et al.* in an article on poly(ethylene terephthalate) with nano-titanium phosphate nanocomposites [46]. In addition to the amorphous halo of rPET, the main diffraction angles of ZrP are highlighted in the rPET/ZrP diffractogram [56]. X-ray diffraction patterns of $rPET/Al(OH)_3/NaPO_2H_2{\cdot}H_2O$ and $PET/ZrPOct/\ Al(OH)_3/NaPO_2H_2{\cdot}H_2O$ pre-

sented a similar profile. The diffractogram showed the amorphous halo of rPET and some diffraction angles of the flame retardants. Similar to FTIR results, by X-ray diffraction the mixing of flame retardant did not reveal apparent chemical interaction among them.

3.5. Thermogravimetry

Figure 9 exhibited the mass loss and derivative curves of the rPET and masterbatches. The rPET and rPET/ZrP curves exhibited only one decay while rPET/$Al(OH)_3$/$NaPO_2H_2{\cdot}H_2O$ and rPET/ZrPOct/$Al(OH)_3$/$NaPO_2H_2.H_2O$ two ones. Although the mass loss and derivatives curves showed very slight fluctuation in the range of 200˚C until T_{onset}, both curves showed quasi imperceptible variations at the same range. The difference of the residues was associated to the flame retardants. Table 2 condensed the values of T_{onset} and T_{max} and residue of each sample. Liu *et al.* investigated the disproportionation of sodium hypophosphite by thermogravimetry [57]. They detected three degradation steps around 310˚C (12.6%), 370˚C (3.5%) and 430˚C (0.5%). Qin *et al.* studied the action of aluminum hydroxide on mechanical properties, flame retardancy and combustion behavior of polypropylene [58]. Thermogravimetry indicated that under nitrogen atmosphere its degradation process occurred at only one step around 230˚C - 350˚C releasing water and generating Al_2O_3. While the onset of degradation was largely unaffected, the retardants did influence the degradation pathway, as evidenced by the significant increase in final residue, a key mechanism of flame retardancy.

3.6. Differential Scanning Calorimetry (DSC)

Figure 10 highlights the three thermal cycles of each sample. For rPET, in the first heating, the glass transition temperature (T_g = 67˚C), the heating crystallization temperature (T_{ch} = 118˚C) and the melting temperature (T_m = 249˚C) were observed. The cooling cycle showed the cooling crystallization temperature (T_{cc} = 214˚C). The last heating cycle presented a melting peak split into two maxima, with T_m = 240 and 249˚C. The rPET/ZrP exhibited two melting peaks (T_m = 245 and 250˚C) at the first heating cycle. When cooling, the crystallization temperature was observed at T_{cc} = 213 °C. Three melting peaks (T_m = 216, 238 and 248˚C) were noticed in the final heating cycle. For the rPET/$Al(OH)_3$/$NaPO_2H_2{\cdot}H_2O$, a T_m at 249˚C was registered during the first heating cycle. The T_{cc} at 217˚C appeared in the cooling cycle. The final heating revealed a T_m at 242˚C. The rPET/ZrPOct/$Al(OH)_3$/$NaPO_2H_2{\cdot}H_2O$ presented a T_g = 97˚C and a T_m = 249˚C in the first heating. After cooling, a T_{cc} was registered at 216˚C. The final heating revealed a T_m at 242˚C. Table 3 summarises the calorimetric data. The rPET/ZrP presented cold crystallization temperature (T_{cc}) and crystallization degree (X_c) like rPET. For rPET/$Al(OH)_3$/$NaPO_2H_2{\cdot}H_2O$ and rPET/ZrPOct/$Al(OH)_3$/$NaPO_2H_2{\cdot}H_2O$, a slight increase in T_{cc} and decrease of crystallization degree were observed probably due to the difficulty of the rPET chains to drive towards the crystallization centers.

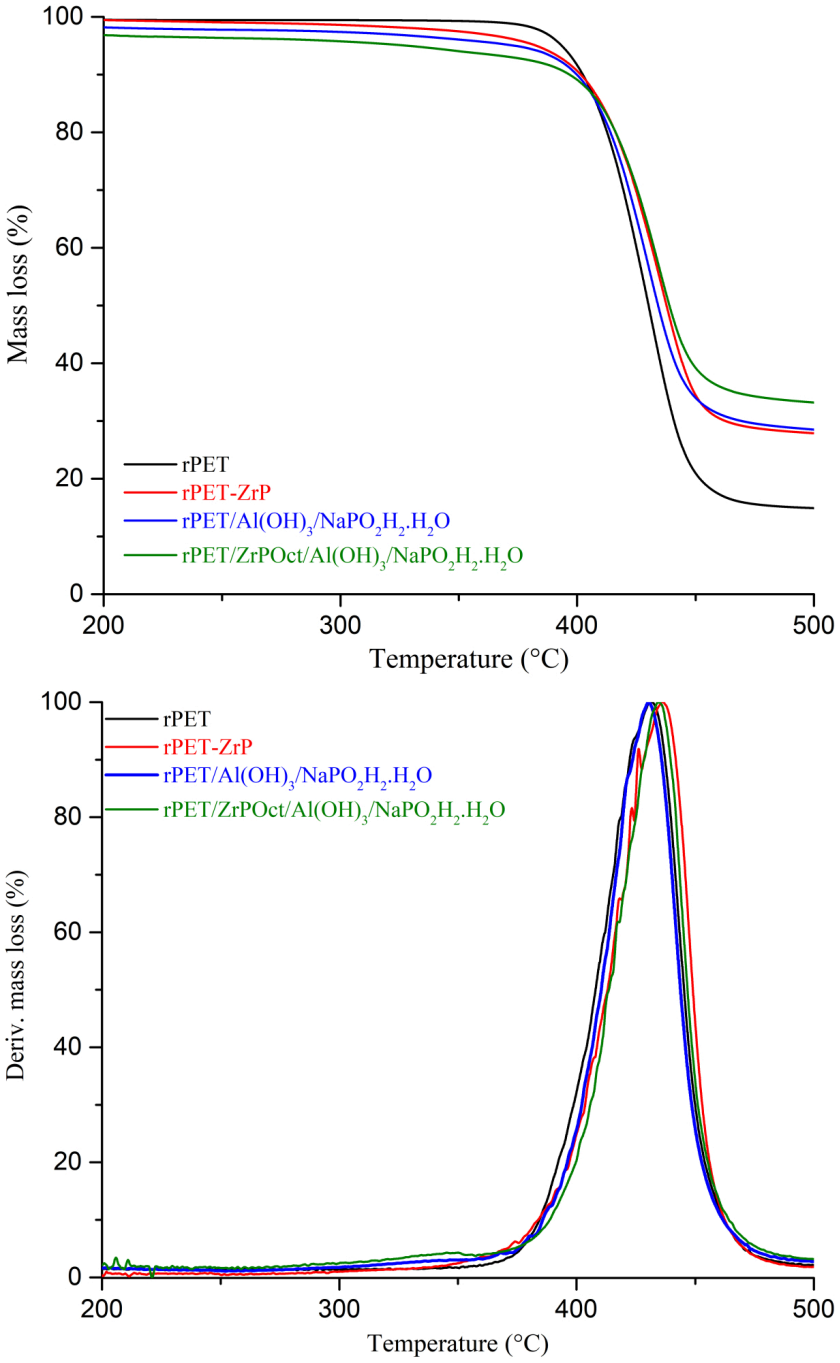

Figure 9. Mass loss and derivative curves of rPET and masterbatches.

Table 2. Thermogravimetric properties of rPET and masterbatches.

Sample	T_{onset}/˚C	T_{max}/˚C	Resdídue/%
rPET	405	432	13
rPET/ZrP	408	436	15
rPET/$Al(OH)_3$/$NaPO_2H_2$·H_2O	406	430	14
rPET/ZrPOct/$Al(OH)_3$/$NaPO_2H_2$·H_2O	406	430	18

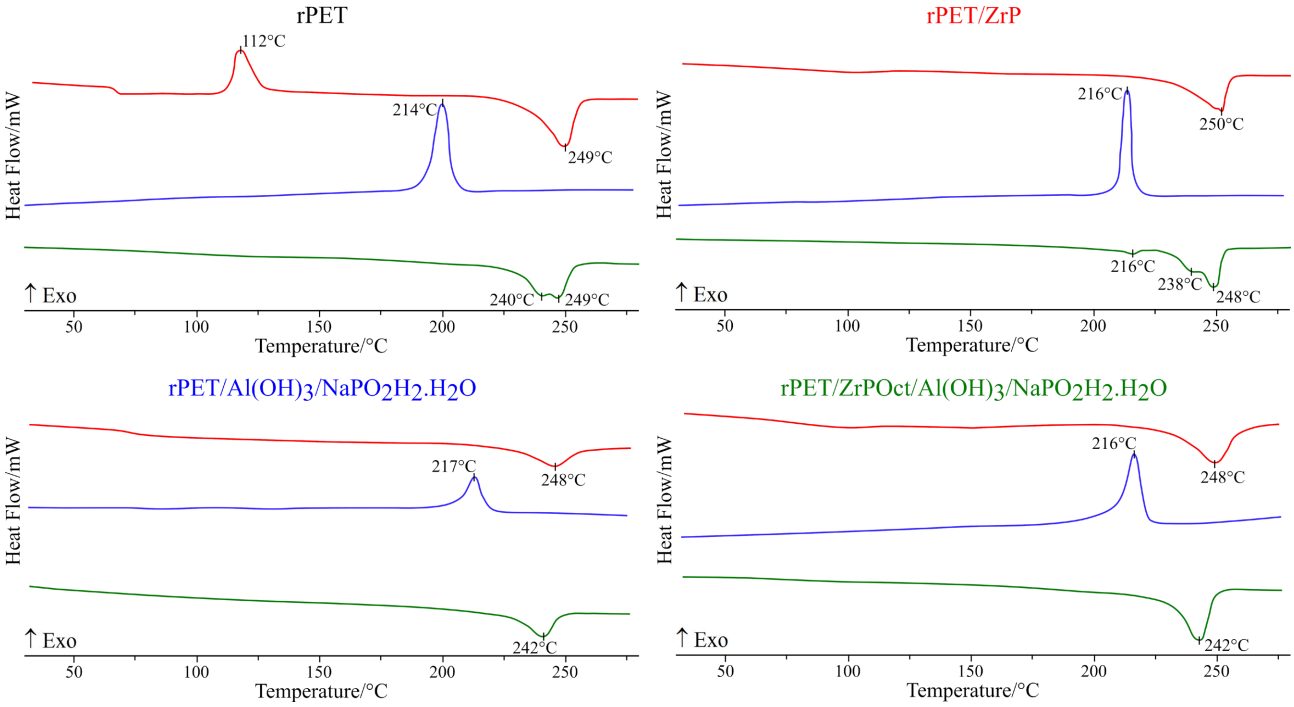

Figure 10. Calorimetric curves of rPET and masterbatches.

Table 3. Samples' T_{cc}, T_m and X_c.

Sample	T_{cc}/°C	T_m^*/°C	X/%
rPET	214	240/249	39
rPET/ZrP	213	216/238/248	38
rPET/$Al(OH)_3$/$NaPO_2H_2$·H_2O	217	242	30
rPET/ZrPOct/$Al(OH)_3$/$NaPO_2H_2$.H_2O	216	242	33

*second heating cycle.

3.7. Rheology

Figure 11 presents the storage (G') and loss (G") moduli and complex viscosity (η*) of the rPET and masterbatches. Bellow 4×10^0 rad s^{-1}, rPET/ZrP showed a quasi-linear behavior with frequency. Above this frequency, an increasing trend was observed, although the values remained lower than those of rPET. The G' for rPET/$Al(OH)_3$/$NaPO_2H_2$·H_2O and rPET/ZrPOct/$Al(OH)_3$/$NaPO_2H_2$·H_2O ZrP showed a quasi-linear behavior with frequency, showing values higher than rPET up to 7.5×10^1 rad s^{-1}. Beyond this frequency, the linear behavior continued but with lower values. In some range of frequency, a slight stiffening can be observed, promoted by the addition of flame retardants. The G" curves of rPET and rPET/ZrP exhibited similar behavior, but lower values were registered for the masterbatch. Around 10^0 rad s^{-1}, the G" curves of rPET/$Al(OH)_3$/$NaPO_2H_2$·H_2O and PET/ZrPOct/$Al(OH)_3$/$NaPO_2H_2$·H_2O tended to linear behavior, with G" values slightly higher than those of rPET. Above this frequency, a continuous increase was noticed, but the values remained lower than those of rPET. Regarding

complex viscosity, rPET showed Newtonian behavior within the investigated frequency range. The rPET/ZrP exhibited pseudoplastic (shear thinning) behavior, showing the lowest viscosity values. The rPET/$Al(OH)_3$/$NaPO_2H_2.H_2O$ and PET/ZrPOct/$Al(OH)_3$/$NaPO_2H_2.H_2O$ complex viscosity curves also showed pseudoplastic (shear thinning) behavior. Around 10^1 rad s^{-1}, the complex viscosity of those samples exhibited different values. Below this frequency, the values were higher than those of rPET, while above it, lower values were registered. Chowreddy *et al.* studied the effect of modified montmorillonite (Cloisite 10A) on the rheological, thermal and mechanical properties of recycled PET. The authors pointed out the dependence of complex viscosity on filler content. Increments in storage and loss moduli were registered from 2 wt.% of filler [59]. Freitas *et al.* investigated the effect of zirconium phosphate (ZrP—1, 2 and 3 wt.%) incorporated into polyamide-6 (PA-6). It was noticed that at the highest ZrP content, the complex viscosity decreased, which was attributed to polymer/polymer and filler/filler interactions [60]. **Figure 12** displays the crossover point of the samples.

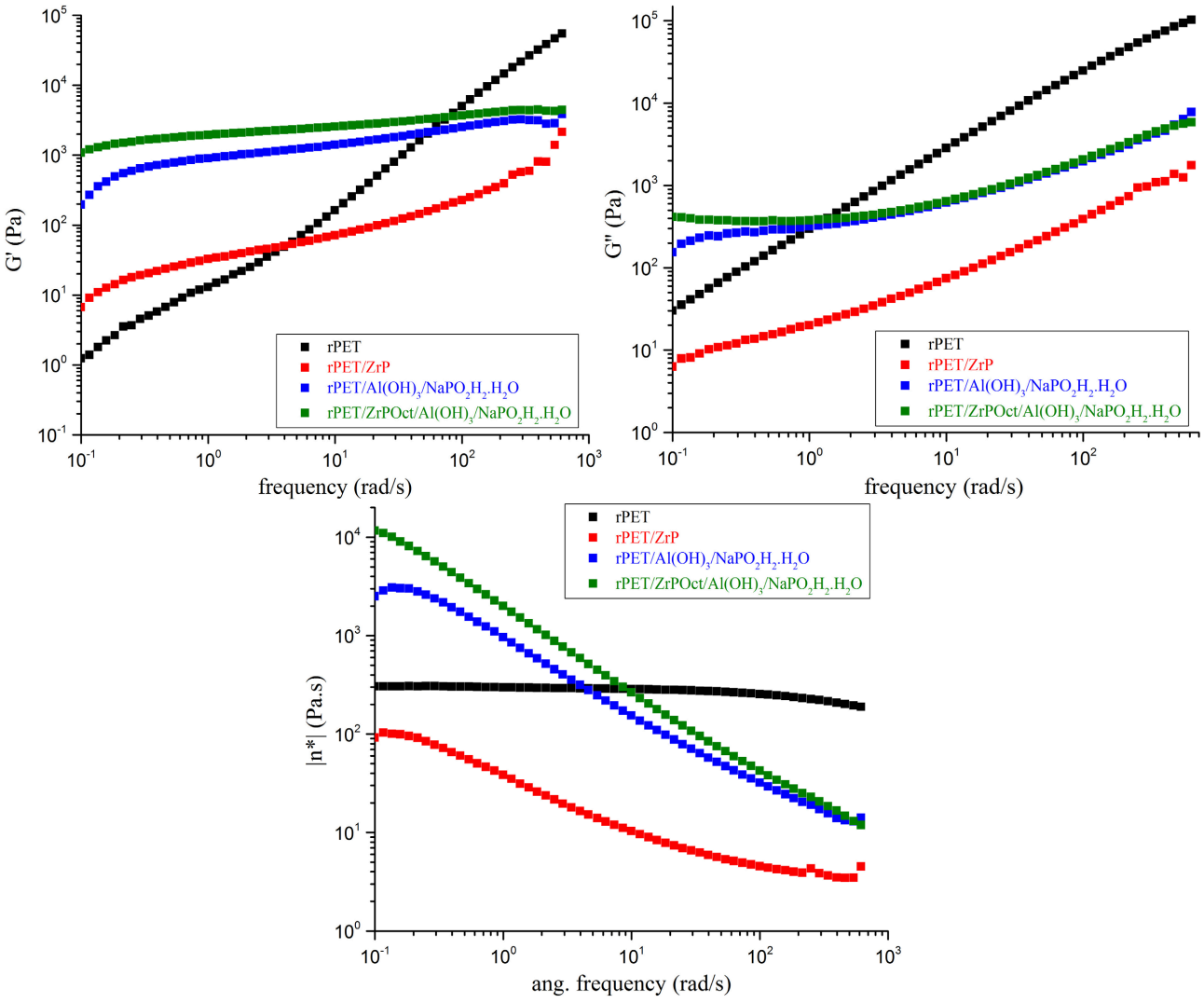

Figure 11. G', G" and complex viscosity curves of rPET and matserbatches.

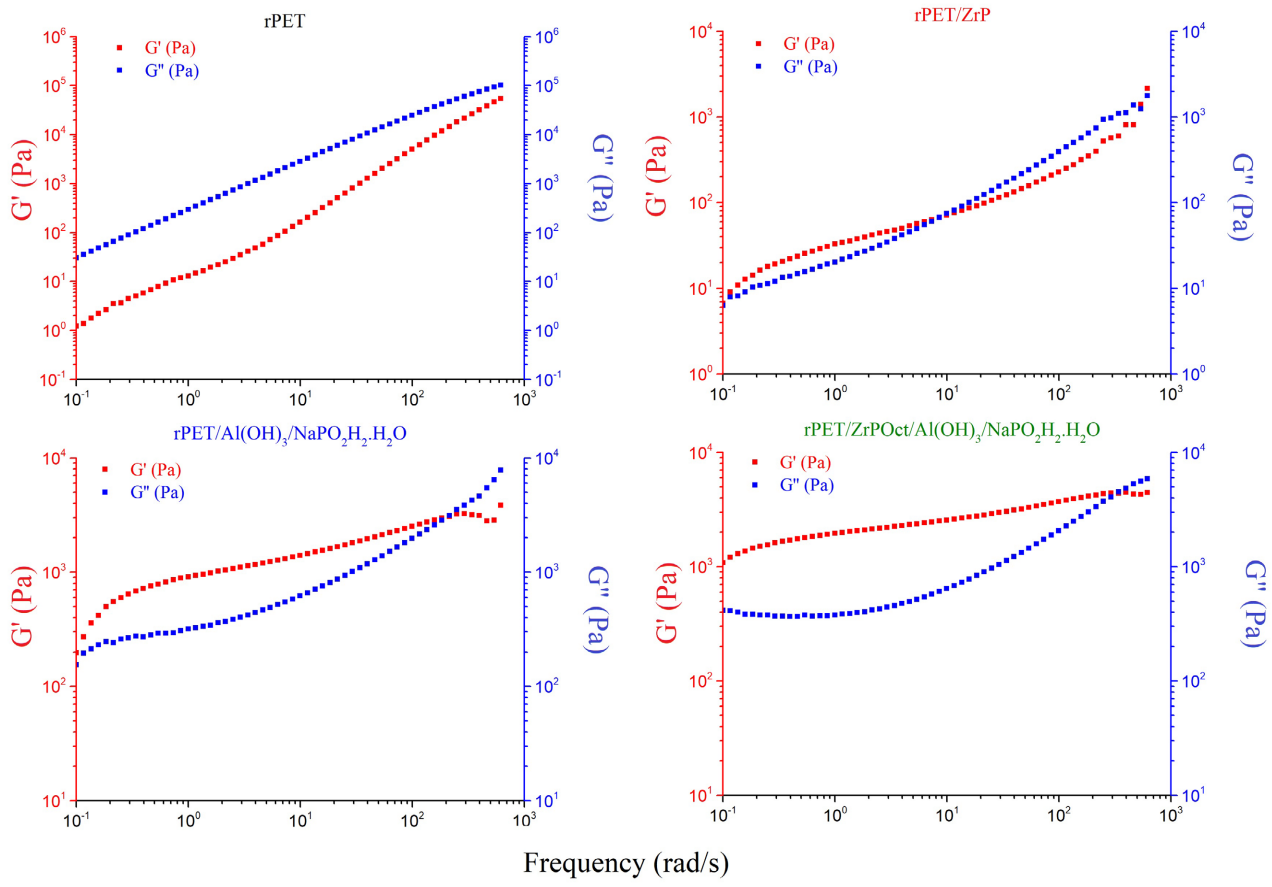

Figure 12. Cross over point of the samples.

Table 4. Crossover point: G"/G' and frequency.

Sample	G"/G'	ang frequency x10²/rad s⁻¹
rPET	-	-
rPET/ZrP	1.08	0.08
	0.99	8.5
rPET/$Al(OH)_3$/$NaPO_2H_2.H_2O$	1.02	2.1
rPET/ZrPOct/$Al(OH)_3$/$NaPO_2H_2.H_2O$	1.03	3.4

The rPET did not present a crossover point within the studied range. The rPET/ZrP presented two crossover points: one around 10^1 rad/s and another in the vicinity of 10^3 rad s^{-1}. The rPET/$Al(OH)_3$/$NaPO_2H_2.H_2O$ and PET/ZrPOct/$Al(OH)_3$/$NaPO_2H_2.H_2O$ showed crossover points between 10^2 - 10^3 rad s^{-1}. In general, when G' was higher than G", the samples showed solid-like behavior, but when G' < G", liquid-like behavior prevailed. Exceptionally, rPET/ZrP seemed to have a second crossover point at a higher frequency, where elastic behavior predominated. Table 4 summarizes the values of the crossover point (G"/G') and frequency of the samples. Simon-Stoger *et al.* examined poly(ethylene tereph-

thalate) waste streams, including selective income (SI), sorting residue (SR), and refuse-derived fuel (RDF) contaminated with organics, to assess the quality of PET waste [61]. Oscillatory rheology was carried out in combination with other analyses. The authors associated the crossover point to each PET waste stream and molecular weight distribution. In summary, they concluded that flame retardants exert a substantial influence on the samples' G', G", complex viscosity, and crossover point. The rPET/$Al(OH)_3$/$NaPO_2H_2.H_2O$ and PET/ZrPOct/$Al(OH)_3$/$NaPO_2H_2.H_2O$ presented similar behaviors, while for rPET/ZrP behaved differently, probably owing to its nanometric dimension. The rheological behavior of the samples is believed to be influenced by the particle dimensions of the flame retardants and the two relaxation regions of rPET.

3.8. Fesem/Eds

Figure 13(a) shows the FESEM/EDS images of the transversal section of the flammability specimen divided into bottom, intermediate, and top portions. For all

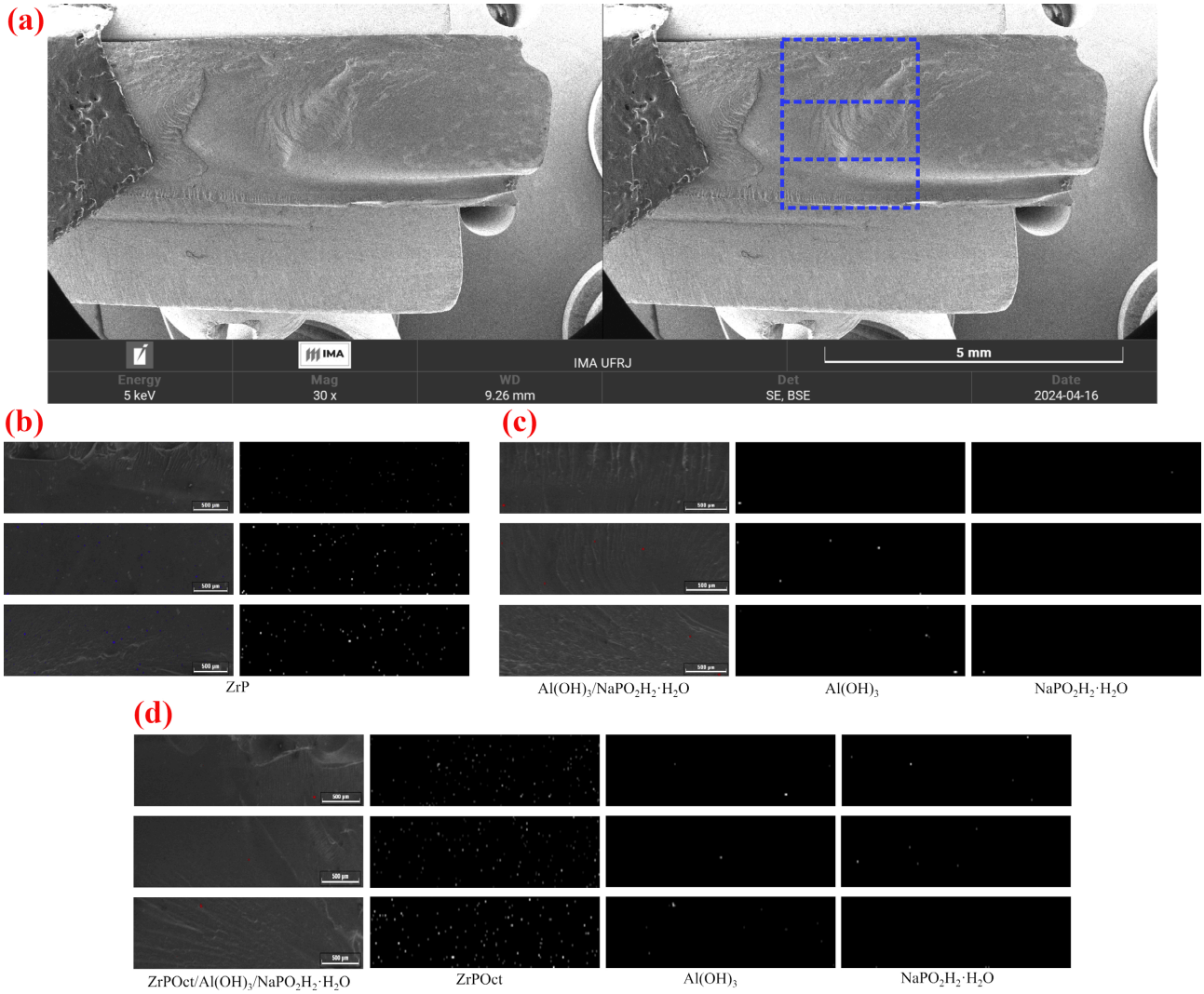

Figure 13. FESEM and EDS of (a) specimen transversal section, (b) FS2, (c) FS3 and (d) FS4.

composites, **Figure 13(b)-(d)** reveal the dispersibility and distribution of the flame retardants within all composites. The left column corresponds to the FESEM image of each specimen from bottom to top. The right columns indicate the dispersibility and distribution of Zr, Al and Na in each composite.

Figure 13(b) (FS2) showed well-dispersed and distributed ZrP particles across the bottom, intermediate, and top regions of the flammability specimen's transverse surface. **Figure 13(c)** (FS3) disclosed the dispersibility and distribution of Al and Na. Both aluminum hydroxide and sodium hypophosphite exhibited poor dispersion and distribution across the bottom, intermediate, and top regions. **Figure 13(d)** (FS4) once again demonstrated that ZrPOct was highly dispersed and distributed. The ZrP seemed to have improved the dispersion and distribution of aluminum hydroxide and sodium hypophosphite, but it was still inadequate. The results reflected the influence of the flame retardants' particle size on their dispersion and distribution within rPET matrix.

3.9. Flammability

Figure 14 depicts the monitoring of the flammability test. From left to right, it shows the burning of the specimen and the dropping of molten material onto the bottom platform. For FS1 (rPET), the specimen burned continuously. The falling drop sustained the flame, and even upon reaching the platform, the flame persisted. For FS2 (rPET/ZrP), immediately after the drop fell, the flame on the specimen extinguished. The drop maintained the flame for a certain time during its fall, but it extinguished before reaching the platform. Specimen FS3 (rPET/$Al(OH)_3$/$NaPO_2H_2.H_2O$) behaved similarly to FS1. The specimen burned continuously. The falling drop kept the flame and even after reaching the platform the flame persisted. Although there was some similarity in behavior with the FS3, the FS4 (rPET/ZrPOct/$Al(OH)_3$/$NaPO_2H_2.H_2O$) showed a tendency toward flame extinction even upon reaching the platform. **Figure 15** presents the images of each specimen after the completion of the flammability test. The images represent, from left to right, the right side view, bottom side view, and left side view, respectively. For all samples, there was no significant warping of the specimens during the test, only a protuberance formed at the bottom of the specimen due to the polymer melting. Wang *et al.* investigated the action of zirconium aminotrimethylene phosphonate (ZrATMP) in the flame retardancy of epoxy resin (EP), registering a significant increase in the char residue. They pointed out that the improvement of flame retardancy and smoke suppression was attributed to the formation of a dense char layer. This char layer acted as a physical barrier, heat insulation, mass exchange and suppressed combustion reactions [62]. **Table 5** discloses dripping speed (drops $5s^{-1}$), flame extinguished time and ignition time of the samples. The sequence for dripping speed and flame extinguishment time is as follows: rPET, rPET/$Al(OH)_3$/$NaPO_2H_2.H_2O$, rPET/ZrPOct/$Al(OH)_3$/$NaPO_2H_2.H_2O$, rPET/ZrP. For ignition time, the sequence is rPET/ZrPOct/$Al(OH)_3$/$NaPO_2H_2.H_2O$, rPET, rPET/$Al(OH)_3$/$NaPO_2H_2.H_2O$, rPET/ZrP. Lessan *et al.* studied the combination of

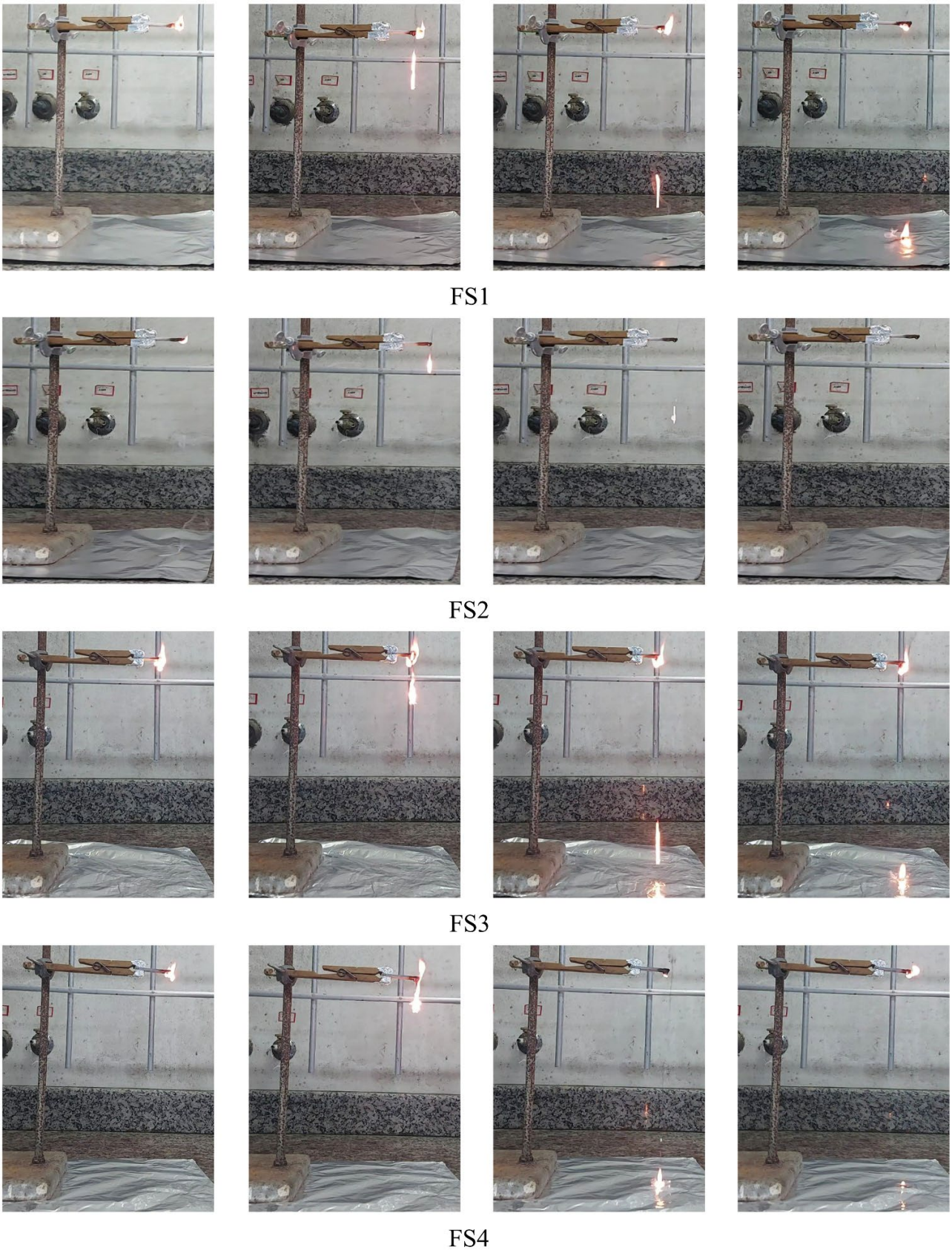

Figure 14. Monitoring of flammability test for rPET (FS1) and composites (FS2, FS3 and FS4).

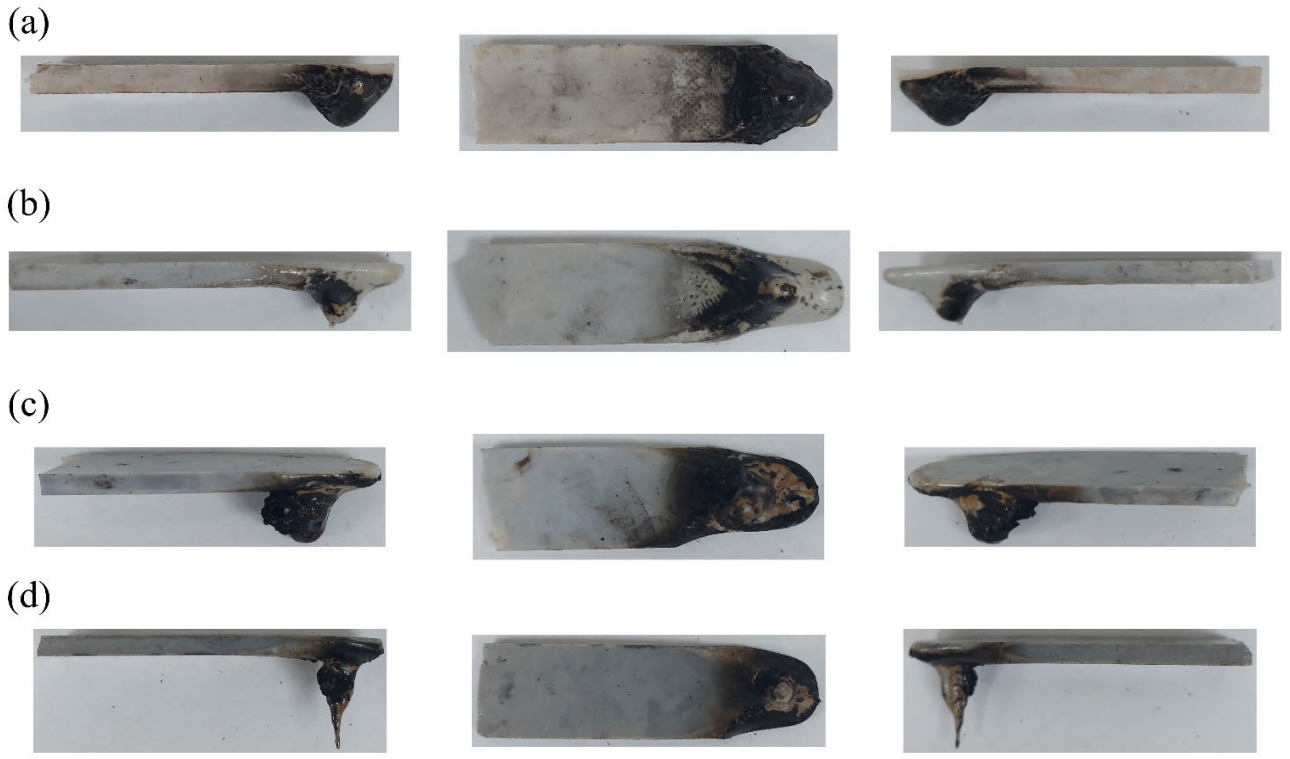

Figure 15. FS appearance after flammability test: (a) FS1, (b) FS2, (c) FS3 and (d) FS4; from left to right: right side view; bottom side view and left side view.

Table 5. Flammability data for rPET and composites.

Sample	Dripping speed/drops $5s^{-1}$	Flame extinguished time/s	Ignition time/s
FS1	4.7 ± 0.6	20.16 ± 0.35	12.25 ± 1.17
FS2	1.0 ± 0	0.78 ± 0.40	10.77 ± 1.86
FS3	4.0 ± 0	10.49 ± 2.49	11.82 ± 2.82
FS4	2.5 ± 0.7	6.94 ± 2.24	13.50 ± 2.00

sodium hypophosphite (SHP), maleic acid (MA), triethanol amine (TEA) and nano TiO_2 as flame retardant. Authors registered that the presence of 5% SHP increased the limit oxygen index from 18.6 to 23 [63]. Goudarzia *et al.* prepared a composite based on poly(vinyl alcohol) with nano-aluminum hydroxide. UL-94 flammability test indicated high flame resistance (V-0). They concluded that the dispersion of the nano-aluminum hydroxide causes some obstruction decreasing the emission of the volatilization product and the thermal transport among polymer decomposition [64]. The results emphasized how the particle size of flame retardants influenced their dispersion and distribution within the rPET matrix. The best findings were shown for ZrP nanoparticles.

4. Conclusion

Post-consumer PET (rPET) from beverage bottles was filled with three different inorganic matters and structural, crystallographic, termal, relaxometry and flam-

mability evaluations were performed. Analysis of the chemical structure did not indicate any chemical interactions among the components. According to NMR, FESEM/EDS, rheology, and flammability tests, the dimension of the flame retardants—nanometric or micrometric—was a crucial factor in their dispersion and distribution inside the rPET matrix. Considering the parameters studied here, the values of dripping speed, flame extinguishment time, and ignition time were particularly relevant for ZrP nanoparticles.

Data Availability Statement

The datasets generated during and/or analyzed during the current study are not publicly available due to the data are not public (Belong to my Institution—Universidade Federal Rio de Janeiro-UFRJ, Brazil).

Acknowledgements

The authors would like to thank the Federal University of Rio de Janeiro (UFRJ), Conselho Nacional de Desenvolvimento Cientifico e Tecnológico (CNPq), Coordenação de Aperfeiçoamento de Pessoal de Nivel Superior (CAPES) Finance Code 1, Fundação Carlos Chagas Filho de Amparo à Pesquisa do Estado do Rio de Janeiro (FAPERJ): processo n˚ E-26/263616/2021; processo E-26/210.032/2024, for supporting this research.

Conflicts of Interest

The authors declare no conflicts of interest regarding the publication of this paper.

References

[1] Murray, A., Skene, K. and Haynes, K. (2015) The Circular Economy: An Interdisciplinary Exploration of the Concept and Application in a Global Context. *Journal of Business Ethics*, **140**, 369-380. https://doi.org/10.1007/s10551-015-2693-2

[2] Korhonen, J., Honkasalo, A. and Seppälä, J. (2018) Circular Economy: The Concept and Its Limitations. *Ecological Economics*, **143**, 37-46. https://doi.org/10.1016/j.ecolecon.2017.06.041

[3] Heyes, G., Sharmina, M., Mendoza, J.M.F., Gallego-Schmid, A. and Azapagic, A. (2018) Developing and Implementing Circular Economy Business Models in Service-Oriented Technology Companies. *Journal of Cleaner Production*, **177**, 621-632. https://doi.org/10.1016/j.jclepro.2017.12.168

[4] Kulas, D.G., Zolghadr, A., Chaudhari, U.S. and Shonnard, D.R. (2023) Economic and Environmental Analysis of Plastics Pyrolysis after Secondary Sortation of Mixed Plastic Waste. *Journal of Cleaner Production*, **384**, Article ID: 135542. https://doi.org/10.1016/j.jclepro.2022.135542

[5] Christopher, F.J., Senthil Kumar, P., Jayaraman, L. and Rangasamy, G. (2023) Assessment of Product Distribution of Plastic Waste from Catalytic Pyrolysis Process. *Fuel*, **332**, Article ID: 126168. https://doi.org/10.1016/j.fuel.2022.126168

[6] Chu, J., Zhou, Y., Cai, Y., Wang, X., Li, C. and Liu, Q. (2023) Flows and Waste Reduction Strategies of PE, PP, and PET Plastics under Plastic Limit Order in China. *Resources, Conservation and Recycling*, **188**, Article ID: 106668.

https://doi.org/10.1016/j.resconrec.2022.106668

[7] Saadeh, D., Al-Khatib, I.A. and Anayah, F.M. (2022) Evaluating Strategies for Sustainable Recovery and Recycling of Plastic Waste in the West Bank of Palestine: The Perspectives of Plastic Companies. *Environmental Monitoring and Assessment*, **195**, Article No. 233. https://doi.org/10.1007/s10661-022-10842-x

[8] Uekert, T., Singh, A., DesVeaux, J.S., Ghosh, T., Bhatt, A., Yadav, G., *et al.* (2023) Technical, Economic, and Environmental Comparison of Closed-Loop Recycling Technologies for Common Plastics. *ACS Sustainable Chemistry & Engineering*, **11**, 965-978. https://doi.org/10.1021/acssuschemeng.2c05497

[9] Jones, H., Saffar, F., Koutsos, V. and Ray, D. (2021) Polyolefins and Polyethylene Terephthalate Package Wastes: Recycling and Use in Composites. *Energies*, **14**, Article 7306. https://doi.org/10.3390/en14217306

[10] Bhanderi, K.K., Joshi, J.R. and Patel, J.V. (2023) Recycling of Polyethylene Terephthalate (PET or PETE) Plastics—An Alternative to Obtain Value Added Products: A Review. *Journal of the Indian Chemical Society*, **100**, Article ID: 100843. https://doi.org/10.1016/j.jics.2022.100843

[11] Ono, S. and Tsusaka, T.W. (2023) Assessing the Selection of PET Recycling Options in Japan: Multi-Criteria Decision Analysis. *Polish Journal of Environmental Studies*, **32**, 4761-4770. https://doi.org/10.15244/pjoes/167400

[12] Shirazimoghaddam, S., Amin, I., Faria Albanese, J.A. and Shiju, N.R. (2023) Chemical Recycling of Used PET by Glycolysis Using Niobia-Based Catalysts. *ACS Engineering Au*, **3**, 37-44. https://doi.org/10.1021/acsengineeringau.2c00029

[13] Giraldo-Narcizo, S., Guenani, N., Sánchez-Pérez, A.M. and Guerrero, A. (2022) Accelerated Polyethylene Terephthalate (PET) Enzymatic Degradation by Room Temperature Alkali Pre-treatment for Reduced Polymer Crystallinity. *ChemBioChem*, **24**, e202200503. https://doi.org/10.1002/cbic.202200503

[14] Pu, M., Zhou, X., Liu, X., Fang, C. and Wang, D. (2023) A Facile, Alternative and Sustainable Feedstock for Transparent Polyurethane Elastomers from Chemical Recycling Waste PET in High-Efficient Way. *Waste Management*, **155**, 137-145. https://doi.org/10.1016/j.wasman.2022.10.032

[15] Ghosh, T., Uekert, T., Walzberg, J., *et al.* (2023) Towards a Circular Economy for PET Bottles in the US. 2023 11*th International Conference on Industrial Ecology* (*ISIE*2023), Leiden, 2-5 July 2023, 1.

[16] Lerna, M., Foti, D., Petrella, A., Sabbà, M.F. and Mansour, S. (2023) Effect of the Chemical and Mechanical Recycling of PET on the Thermal and Mechanical Response of Mortars and Premixed Screeds. *Materials*, **16**, Article 3155. https://doi.org/10.3390/ma16083155

[17] Roungpaisan, N., Srisawat, N., Rungruangkitkrai, N., Chartvivatpornchai, N., Boonyarit, J., Kittikorn, T., *et al.* (2023) Effect of Recycling PET Fabric and Bottle Grade on R-Pet Fiber Structure. *Polymers*, **15**, Article 2330. https://doi.org/10.3390/polym15102330

[18] Bocz, K., Ronkay, F., Vadas, D., Molnár, B., Gere, D., Czigány, T., *et al.* (2022) Flame Retardancy of PET Foams Manufactured from Bottle Waste. *Journal of Thermal Analysis and Calorimetry*, **148**, 217-228. https://doi.org/10.1007/s10973-022-11423-3

[19] Ahmed, L., Zhang, B., Hatanaka, L.C. and Mannan, M.S. (2018) Application of Polymer Nanocomposites in the Flame Retardancy Study. *Journal of Loss Prevention in the Process Industries*, **55**, 381-391. https://doi.org/10.1016/j.jlp.2018.07.005

[20] Feng, J., Liu, L., Zhang, Y., Wang, Q., Liang, H., Wang, H., *et al.* (2023) Rethinking the Pathway to Sustainable Fire Retardants. *Exploration*, **3**, Article ID: 20220088. https://doi.org/10.1002/exp.20220088

[21] Iqbal, M.A., Iqbal, M.A. and Fedel, M. (2018) Fire Retardancy of Aluminum Hydroxide Reinforced Flame Retardant Modified Epoxy Resin Composite. *Russian Journal of Applied Chemistry*, **91**, 680-686. https://doi.org/10.1134/s1070427218040225

[22] Ai, L., Chen, S., Yang, L. and Liu, P. (2021) Synergistic Flame Retardant Effect of Organic Boron Flame Retardant and Aluminum Hydroxide on Polyethylene. *Fibers and Polymers*, **22**, 354-365. https://doi.org/10.1007/s12221-021-9385-6

[23] Shi, J., Zeng, W., Yang, Z., Li, J., Zhao, P., Li, H., *et al.* (2021) Effect of Particle Size on Flame Retardancy and Mechanical Properties of Hydroxyethyl Diphosphate Modified Aluminum Hydroxide Intrinsic Polyethylene Terephthalate. *Journal of Applied Polymer Science*, **138**, e50500. https://doi.org/10.1002/app.50500

[24] Park, S.Y., Park, E.J., Lee, M.Y., Park, C., Kim, H.G., Jeong, E.D., *et al.* (2008) Preparation of $Al(OH)_3$/PMMA Nanocomposites by Emulsion Polymerization. *Polymers for Advanced Technologies*, **19**, 1803-1808. https://doi.org/10.1002/pat.1197

[25] Yang, W., Song, L., Hu, Y., Lu, H. and Yuen, R.K.K. (2011) Enhancement of Fire Retardancy Performance of Glass-Fibre Reinforced Poly(Ethylene Terephthalate) Composites with the Incorporation of Aluminum Hypophosphite and Melamine Cyanurate. *Composites Part B*: *Engineering*, **42**, 1057-1065. https://doi.org/10.1016/j.compositesb.2011.03.019

[26] Zheng, J., Wang, C., Zhao, Y., Guo, M., He, Y. and Xin, C. (2023) The Synergy of Nanosilica and Zinc Diethyl Hypophosphite Influences the Flame Retardancy and Foaming Performance of Poly(Ethylene Terephthalate). *Advances in Polymer Technology*, **2023**, Article ID: 4319998. https://doi.org/10.1155/2023/4319998

[27] Yang, W., Tang, G., Song, L., Hu, Y. and Yuen, R.K.K. (2011) Effect of Rare Earth Hypophosphite and Melamine Cyanurate on Fire Performance of Glass-Fiber Reinforced Poly(1, 4-Butylene Terephthalate) Composites. *Thermochimica Acta*, **526**, 185-191. https://doi.org/10.1016/j.tca.2011.09.022

[28] Wu, X.L. and Yang, C.Q. (2008) Flame Retardant Finishing of Cotton Fleece Fabric: Part III—The Combination of Maleic Acid and Sodium Hypophosphite. *Journal of Fire Sciences*, **26**, 351-368. https://doi.org/10.1177/0734904108090732

[29] Albitres, G., Garcia, E., Soares, C., Freitas, D., Neto, R.C. and Mendes, L. (2024) Post-consumer High Density Polyethylene/Zirconium Phosphate and Aluminum Hydroxide Composites: Assessment of Physico-Mechanical and Flame Retardancy Properties. *Journal of Composite Materials*, **58**, 489-503. https://doi.org/10.1177/00219983231226278

[30] Mendes, L.C., Mariano, D.M., Freitas, D.F.S., Albitres, G.A.V., Tavares, M.I.B. and Garcia, E.E. (2024) Ecofriendly Composites Based on Poly (Lactic Acid) with Nano-Zirconium Phosphate and Nano-Zinc Oxide/Zirconium Phosphate: Physicochemical and Aging Characteristics. *Journal of Thermal Analysis and Calorimetry*, **149**, 9297-9306. https://doi.org/10.1007/s10973-024-13541-6

[31] Mendes, L.C., Silva, D.F., Araujo, L.J.F. and Lino, A.S. (2014) Zirconium Phosphate Organically Intercalated/Exfoliated with Long Chain Amine. *Journal of Thermal Analysis and Calorimetry*, **118**, 1461-1469. https://doi.org/10.1007/s10973-014-4056-0

[32] (2021) ASTM D3418, Standard Test Method for Transition Temperatures and Enthalpies of Fusion and Crystallization of Polymers by Differential Scanning Calorimetry. ASTM International. https://www.astm.org/d3418-21.html

[33] Chowreddy, R.R., Nord-Varhaug, K. and Rapp, F. (2018) Recycled Polyethylene Terephthalate/Carbon Nanotube Composites with Improved Processability and Performance. *Journal of Materials Science*, **53**, 7017-7029. https://doi.org/10.1007/s10853-018-2014-0

[34] (2022) ASTM D635-22. Standard Test Method for Rate of Burning and/or Extent and Time of Burning of Plastics in a Horizontal Position. ASTM International. https://www.astm.org/d0635-22.html

[35] Mathew, X. and Nayar, V.U. (1988) Vibrational Spectra of Three Zirconium Phosphates. *Infrared Physics*, **28**, 189-194. https://doi.org/10.1016/0020-0891(88)90009-7

[36] Casciola, M., Donnadio, A., Montanari, F., Piaggio, P. and Valentini, V. (2007) Vibrational Spectra and H-Bondings in Anhydrous and Monohydrate α-Zr Phosphates. *Journal of Solid State Chemistry*, **180**, 1198-1208. https://doi.org/10.1016/j.jssc.2007.01.016

[37] Bian, Y., Bai, M., Cao, J. and Li, J. (2023) A Strong Soybean Meal Adhesive Enhanced by Aluminum Hydroxide Nanoparticles via a Low-Cost and Simple Organic-Inorganic Hybrid Strategy. *International Journal of Adhesion and Adhesives*, **125**, Article ID: 103442. https://doi.org/10.1016/j.ijadhadh.2023.103442

[38] Riesgraf, D.A. and May, M.L. (1978) Infrared Spectra of Aluminum Hydroxide Chlorides. *Applied Spectroscopy*, **32**, 362-366. https://doi.org/10.1366/000370278774331233

[39] Demichelis, R., Noël, Y., Ugliengo, P., Zicovich-Wilson, C.M. and Dovesi, R. (2011) Physico-Chemical Features of Aluminum Hydroxides as Modeled with the Hybrid B3LYP Functional and Localized Basis Functions. *The Journal of Physical Chemistry C*, **115**, 13107-13134. https://doi.org/10.1021/jp200523x

[40] Frost, R.L., Kloprogge, J.T., Russell, S.C. and Szetu, J.L. (1999) Vibrational Spectroscopy and Dehydroxylation of Aluminum (Oxo)Hydroxides: Gibbsite. *Applied Spectroscopy*, **53**, 423-434. https://doi.org/10.1366/0003702991946884

[41] Schramm, C., Rinderer, B., Binder, W.H., Tessadri, R. and Duelli, H. (2007) Novel Sol-Gel Derived Cellular Foam: Reaction of an Organotrialkoxysilane with Sodium Hypophosphite. *Journal of Sol-Gel Science and Technology*, **45**, 83-88. https://doi.org/10.1007/s10971-007-1627-6

[42] Noisong, P. and Danvirutai, C. (2010) A New Synthetic Route, Characterization and Vibrational Studies of Manganese Hypophosphite Monohydrate at Ambient Temperature. *Spectrochimica Acta Part A: Molecular and Biomolecular Spectroscopy*, **77**, 890-894. https://doi.org/10.1016/j.saa.2010.08.028

[43] Wu, W., Lv, S., Liu, X., Qu, H., Zhang, H. and Xu, J. (2014) Using TG-FTIR and TG-MS to Study Thermal Degradation of Metal Hypophosphites. *Journal of Thermal Analysis and Calorimetry*, **118**, 1569-1575. https://doi.org/10.1007/s10973-014-4085-8

[44] (2017) Sodium Hypophosphite Monohydrate (10039-56-2) IR1. https://www.chemicalbook.com/SpectrumEN_10039-56-2_ir1.htm

[45] Tanner, P.A., Sze, T., Mak, T.C. and Yip, W. (1992) Synthesis, Crystal Structure and Vibrational Spectra of Uranium(IV) Hypophosphite. *Journal of Crystallographic and Spectroscopic Research*, **22**, 25-30. https://doi.org/10.1007/bf01161359

[46] Valencia Albitres, G.A., Cestari, S.P., Malafaia Macedo, K.R., Mendes, L.C., Cruz, M.O., Filho, M.F., *et al.* (2019) Poly(Ethylene Terephthalate)/Titanium Phosphate Nanocomposites: Effect of Fillers on Thermal, Crystallographic Diffraction, Molecular Mobility, and UV-Vis Absorption. *Journal of Thermoplastic Composite Materials*, **35**, 891-909. https://doi.org/10.1177/0892705719886926

[47] Mendiburu-Valor, E., Mondragon, G., González, N., Kortaberria, G., Martin, L., Eceiza, A., *et al.* (2022) Valorization of Urban and Marine PET Waste by Optimized Chemical Recycling. *Resources, Conservation and Recycling*, **184**, Article ID: 106413. https://doi.org/10.1016/j.resconrec.2022.106413

[48] Pereira, A.P.D.S., Silva, M.H.P.D., Lima Júnior, É.P., Paula, A.D.S. and Tommasini, F.J. (2017) Processing and Characterization of PET Composites Reinforced with Geopolymer Concrete Waste. *Materials Research*, **20**, 411-420. https://doi.org/10.1590/1980-5373-mr-2017-0734

[49] He, X., Xiao, H., Choi, H., Díaz, A., Mosby, B., Clearfield, A., *et al.* (2014) *α*-Zirconium Phosphate Nanoplatelets as Lubricant Additives. *Colloids and Surfaces A: Physicochemical and Engineering Aspects*, **452**, 32-38. https://doi.org/10.1016/j.colsurfa.2014.03.041

[50] Tsuboi, M. (1957) Vibrational Spectra of Phosphite and Hypophosphite Anions, and the Characteristic Frequencies of PO_3^- and PO_2^- Groups. *Journal of the American Chemical Society*, **79**, 1351-1354. https://doi.org/10.1021/ja01563a026

[51] Darkhalil, I.D., Nagels, N., Herrebout, W.A., van der Veken, B.J., Gurusinghe, R.M., Tubergen, M.J., *et al.* (2014) Microwave Spectra and Conformational Studies of Ethylamine from Temperature Dependent Raman Spectra of Xenon Solutions and Ab Initio Calculations. *Journal of Molecular Structure*, **1068**, 101-111. https://doi.org/10.1016/j.molstruc.2014.03.073

[52] Bistričić, L., Borjanović, V., Leskovac, M., Mikac, L., McGuire, G.E., Shenderova, O., *et al.* (2015) Raman Spectra, Thermal and Mechanical Properties of Poly(Ethylene Terephthalate) Carbon-Based Nanocomposite Films. *Journal of Polymer Research*, **22**, Article No. 39. https://doi.org/10.1007/s10965-015-0680-z

[53] Zhu, C., Tong, N., Song, L. and Zhang, G. (2015) Investigation of Raman Spectra of Polyethylene Terephthalate. *SPIE Proceedings*, **9656**, 72-76. https://doi.org/10.1117/12.2205157

[54] Peñalver, R., Zapata, F., Arroyo-Manzanares, N., López-García, I. and Viñas, P. (2022) Raman Spectroscopic Strategy for the Discrimination of Recycled Polyethylene Terephthalate in Water Bottles. *Journal of Raman Spectroscopy*, **54**, 107-112. https://doi.org/10.1002/jrs.6457

[55] Rodrigues, E.J.D.R., Cavalcante, M.D.P. and Tavares, M.I.B. (2016) Time Domain NMR Evaluation of Poly(Vinyl Alcohol) Xerogels. *Polímeros*, **26**, 221-227. https://doi.org/10.1590/0104-1428.2093

[56] Brandão, L.S., Mendes, L.C., Medeiros, M.E., Sirelli, L. and Dias, M.L. (2006) Thermal and Mechanical Properties of Poly(Ethylene Terephthalate)/Lamellar Zirconium Phosphate Nanocomposites. *Journal of Applied Polymer Science*, **102**, 3868-3876. https://doi.org/10.1002/app.24096

[57] Liu, D., Li, X., Wei, L., Zhang, T., Wang, A., Liu, C., *et al.* (2017) Disproportionation of Hypophosphite and Phosphite. *Dalton Transactions*, **46**, 6366-6378. https://doi.org/10.1039/c7dt00243b

[58] Qin, Z., Li, D., Li, Q. and Yang, R. (2016) Effect of Nano-Aluminum Hydroxide on Mechanical Properties, Flame Retardancy and Combustion Behavior of Intumescent Flame Retarded Polypropylene. *Materials & Design*, **89**, 988-995. https://doi.org/10.1016/j.matdes.2015.10.007

[59] Chowreddy, R.R., Nord-Varhaug, K. and Rapp, F. (2018) Recycled Poly(Ethylene Terephthalate)/Clay Nanocomposites: Rheology, Thermal and Mechanical Properties. *Journal of Polymers and the Environment*, **27**, 37-49.

https://doi.org/10.1007/s10924-018-1320-6

[60] Freitas, D.D.F.D.S., Albitres, G.A.V., Mariano, D.D.M., Cestari, S.P. and Mendes, L.C. (2022) Mechanical, Thermal, Rheological Assessment of Polyamide-6 Reinforced Composites by Addition of Lamellar Zirconium Phosphate. *Journal of Thermoplastic Composite Materials*, **36**, 2600-2622. https://doi.org/10.1177/08927057221102858

[61] Simon-Stőger, L., Kovács, A., Szigeti, M., Bobek-Nagy, J., Kurdi, R. and Varga, C. (2024) Oscillation Rheology, Calorimetry and Computed Tomography: A Practical Toolkit Combination of Qualification for Real Poly(Ethylene Terephthalate) Waste. *Journal of Cleaner Production*, **454**, 142346. https://doi.org/10.1016/j.jclepro.2024.142346

[62] Wang, X., Zhang, J., Fu, X., Chu, F. and Hu, Y. (2024) Synthesis of Zirconium Aminotrimethylene Phosphonate Nanorods and Their Application in Toughened and Flame Retarded Epoxy Composites. *Composites Part A*: *Applied Science and Manufacturing*, **179**, Article ID: 108059. https://doi.org/10.1016/j.compositesa.2024.108059

[63] Lessan, F., Montazer, M. and Moghadam, M.B. (2011) A Novel Durable Flame-Retardant Cotton Fabric Using Sodium Hypophosphite, Nano TiO_2 and Maleic Acid. *Thermochimica Acta*, **520**, 48-54. https://doi.org/10.1016/j.tca.2011.03.012

[64] Goudarzia, M., Ghanbarib, D. and Salavati-Niasaria, M. (2015) Room Temperature Preparation of Aluminum Hydroxide Nanoparticles and Flame Retardant Poly Vinyl Alcohol Nanocomposite. *Journal of Nanostructure*, **5**, 110-115. https://doi.org/10.7508/jns.2015.02.005